






Anti-hsa-miR-59 alleviates premature senescence associated with Hutchinson-Gilford progeria syndrome in mice

Qianying Hu^{1,†} , Na Zhang^{1,†}, Tingting Sui², Guanlin Li³, Zhiyao Wang¹, Mingyue Liu³, Xiaojuan Zhu¹ , Baiqu Huang¹, Jun Lu^{3,*} , Zhanjun Li^{2,**}  & Yu Zhang^{1,***} 

Abstract

Hutchinson-Gilford progeria syndrome (HGPS) is a lethal premature aging disorder without an effective therapeutic regimen. Because of their targetability and influence on gene expression, microRNAs (miRNAs) are attractive therapeutic tools to treat diseases. Here we identified that hsa-miR-59 (miR-59) was markedly upregulated in HGPS patient cells and in multiple tissues of an HGPS mouse model (*Lmna*^{G609G/G609G}), which disturbed the interaction between RNAPII and TFIID, resulting in abnormal expression of cell cycle genes by targeting high-mobility group A family HMGA1 and HMGA2. Functional inhibition of miR-59 alleviated the cellular senescence phenotype of HGPS cells. Treatment with AAV9-mediated anti-miR-59 reduced fibrosis in the quadriceps muscle, heart, and aorta, suppressed epidermal thinning and dermal fat loss, and yielded a 25.5% increase in longevity of *Lmna*^{G609G/G609G} mice. These results identify a new strategy for the treatment of HGPS and provide insight into the etiology of HGPS disease.

Keywords HGPS; HMGA; miR-59; TFIID

Subject Categories Cell Cycle; Genetics, Gene Therapy & Genetic Disease; Molecular Biology of Disease

DOI 10.15252/emboj.2022110937 | Received 15 February 2022 | Revised 27 September 2022 | Accepted 29 September 2022 | Published online 16 November 2022

The EMBO Journal (2023) 42: e110937

Introduction

Hutchinson-Gilford progeria syndrome (HGPS) is the most common and severe form of a premature aging syndrome (Battista *et al.*, 2003; Gonzalo *et al.*, 2017). Children usually appear healthy at birth, age rapidly during childhood, and most die of myocardial infarction or stroke at an average age of 14.6 years (Gordon

et al., 2014a; Prakash *et al.*, 2018). Over 90% cases result from a single *de novo* point and dominant mutation of LMNA gene (c.1824 C > T; p.Gly608Gly) that activates a cryptic splice site in exon 11 and produces a truncated lamin A (progerin) (Eriksson *et al.*, 2003; Liu *et al.*, 2005). The progerin remains farnesylated, thus inducing morphologic alterations of the nuclear envelope and impaired cellular functions, such as genomic stability, epigenetic regulation of miRNA and gene expression, protein and energy metabolism, and nucleocytoplasmic transport (Jung *et al.*, 2012; Nissan *et al.*, 2012; Gordon *et al.*, 2014b; Buchwalter & Hetzer, 2017; Gonzalo *et al.*, 2017; Kubben & Misteli, 2017).

Various attempts have been made to alleviate progeria symptoms, but the only FDA-approved drug for HGPS is lonafarnib, an orally active FTase inhibitor. Lonafarnib inhibits farnesyltransferase to prevent farnesylation and subsequent accumulation of progerin, then extends patients' lives by about 2.5 years. Lonafarnib, however, is still limited in terms of large quantities of applications by adverse reactions, such as vomiting, diarrhea, infection, nausea, and fatigue, which results in the presence of progerin that has not been released from the nuclear membrane. In addition, the effect of released progerin by lonafarnib is unclear (Dhillon, 2021). Meanwhile, there are other attempts for HGPS therapy. A clinical trial is underway with everolimus (rapamycin analogs) to facilitate lysosomal degradation of progerin by activating autophagy (Cao *et al.*, 2011). In addition, several gene editing-based strategies aimed at reducing progerin have been developed, which prolong longevity of HGPS mice in varying degrees (Beyret *et al.*, 2019; Santiago-Fernández *et al.*, 2019; Erdos *et al.*, 2021; Puttaraju *et al.*, 2021). However, due to many limitations, there is still a long way to clinical application. Therefore, there is an urgent need to develop new therapeutic techniques for HGPS.

microRNAs (miRNAs) are powerful regulators of gene expression that mainly function by degrading target mRNAs or inhibiting their translation (Bartel, 2004). In recent years, miRNAs have become useful tools and targets for novel therapeutic approaches in multiple

1 The Key Laboratory of Molecular Epigenetics of the Ministry of Education (MOE), Northeast Normal University, Changchun, China

2 The Key Laboratory of Zoonosis Research, Ministry of Education, College of Animal Science, Jilin University, Changchun, China

3 The Institute of Genetics and Cytology, Northeast Normal University, Changchun, China

*Corresponding author. Tel: +86 431 85099798; E-mail: luj809@nenu.edu.cn

**Corresponding author. Tel: +86 431 87836151; E-mail: lizj_1998@jlu.edu.cn

***Corresponding author. Tel: +86 431 85098729; E-mail: zhangy288@nenu.edu.cn

†These authors contributed equally to this work

diseases, including cardiovascular diseases, cancer, hepatitis C, and type 2 diabetes (Jopling *et al*, 2005; Calin *et al*, 2008; Cheng & Zhang, 2010; Roggli *et al*, 2012; Ling *et al*, 2013; Luna *et al*, 2015; Rupaimoole & Slack, 2017). However, few miRNAs have been reported to exert protective effects in progeria. miR-9, a brain-specific miRNA, is the major regulator of lamin A expression, which explains the absence of neuronal disorders in HGPS patients by preventing progerin accumulation and its associated toxic effects (Jung *et al*, 2012; Nissan *et al*, 2012). In addition, several miRNAs have been reported in a Zmpste24-deficient mouse model (Zmpste24^{-/-}), a mouse model for simulating HGPS and associated syndromes linked to prenylated prelamin A accumulation (Pendás *et al*, 2002). Four miRNAs (the miR-29 family, miR-1, miR-342-5p, and miR-365) have significant roles in Zmpste24^{-/-} cells (Mariño *et al*, 2010; Maurer *et al*, 2010; Ugalde *et al*, 2011; Xiong *et al*, 2015; Zhang *et al*, 2017). Upregulated miR-29 reduces cell proliferation and induces cell senescence (Maurer *et al*, 2010). miR-1 is upregulated in Zmpste24^{-/-} mouse livers and fibroblasts of patients with HGPS. miR-1 represses insulin-like growth factor (IGF-1) and contributes to somatotroph axis repression (Mariño *et al*, 2010). However, studies on functional miRNAs that can regulate HGPS senescence are lacking. Thus, it is important to determine whether miRNAs can be used as therapeutic targets for HGPS.

In the current study, has-miR-59 (miR-59) was identified in an miRNA sequencing project as upregulated when overexpression progerin. After inhibiting miR-59, we conducted experiments to determine how miR-59 regulates HGPS cellular senescence by targeting HMGAs. Moreover, AAV9-anti-miR-59 was delivered to *Lmna*^{G609G/G609G} mice to assess the possibility as a therapeutic drug by detecting the aging phenotype and longevity of HGPS mice.

Results

A novel miRNA, miR-59 promotes HGPS cellular senescence

To identify the most effective miRNA for HGPS, we used a lentiviral-based system to express Flag-tagged progerin in human skin fibroblast CRL-1474 cells to model the pathophysiology of HGPS fibroblasts. As measured by biomarkers of cellular

senescence, progerin expression led to premature senescence (Fig EV1A and B). Then, we performed miRNA-seq between progerin-expressing CRL-1474 and control cells, which showed that progerin induced notable changes in miRNA expression (Fig 1A and B). miR-3656 and miR-59 were the two most prominent miRNAs among the top 10 upregulated miRNAs in HGPS fibroblasts (Fig 1C and D). We then synthesized antagonists (anti-miR-3656 and anti-miR-59) to inhibit the endogenous activity of the miRNAs. Anti-miR-3656 or anti-miR-59 remarkably reduced (SA)-β-gal-positive cells, restored proliferative capacity, and increased the expression of cyclin A2 and lamin B1 in HGPS patient cells. Anti-miR-59 was shown to be more effective than anti-miR-3656 in alleviating cellular senescence (Figs 1E–G and EV1C). Similarly, anti-miR-59 alleviated progerin-expressing CRL-1474 and IMR90 fibroblast senescence (Figs 1H–J and EV1D–F). Thus, we decided to focus on miR-59 for an intensive study of the roles and mechanisms of action.

Premature senescence of HGPS is equivalent to an accelerated version of physiologic senescence (Cenni *et al*, 2020). This finding prompted us to determine whether miR-59 is also increased in physiologic human fibroblast senescence. We observed a marked upregulation of miR-59 in fibroblasts derived from 88- and 92-year-old individuals compared with the 7-year-old cells (CRL-1474) (Fig 1K). Treatment with anti-miR-59 increased cyclin A2 and lamin B1 levels, the proportion of Ki67positive cells, and reduced (SA)-β-gal-positive cells in 88-year-old cells (Figs 1L and EV1G–H). In addition, upregulated miR-59 was also detected in replicative senescence cells (Fig EV1G). Therefore, it appeared that anti-miR-59 alleviated HGPS cellular senescence and physiologic aging.

HMGA1 and HMGA2 are target genes of miR-59

To determine the specific role of miR-59 during HGPS cellular senescence, we identified the direct target genes of miR-59. We used TargetScan and miRanda software to predict 867 putative target genes of miR-59. Then, we performed GO analysis of the 867 putative target genes. Seven potential target genes associated with aging were elaborated (Fig 2A). Treatment of HGPS patient cells with anti-miR-59 upregulated mRNA levels of the seven potential target genes, among which HMGA1 and HMGA2 were the most significantly upregulated genes (Fig 2B and C). Similarly, anti-miR-59 also

Figure 1. Identifying a new-found miRNA, miR-59 during HGPS cellular senescence.

- A A heatmap showing the differential miRNAs expression as determined by miRNA-seq in progerin-expressing cells relative to control cells, $P < 0.05$. Lowly expressed miRNAs were shown in blue, highly expressed ones in red.
- B Volcano Plot of top 10 miRNAs upregulated and two miRNAs downregulated in HGPS cells compared with control.
- C The level of top 10 upregulated miRNAs in HGPS cells was assessed by qPCR.
- D The level of novel-miR-27, miR-3656, and miR-59 in HGPS patient cells (HGAFDFN003 p21 and HGAFDFN167 p19) versus control (CRL-1474 cells p28) was assessed by qPCR.
- E–G HGAFDFN003 cells were transfected with anti-miR-ctrl, anti-miR-3656, or anti-miR-59 for 5 days, cells were subjected to SA-β-gal staining. The percentage of SA-β-gal positive cells was calculated. Scale bars: 100 μm (E). The percentage of the Ki67 positive cells was calculated by immunofluorescence (F). The level of cyclin A2 and lamin B1 was detected by Western blot (G).
- H–J Progerin-expressing CRL-1474 cells were transfected with anti-miR-ctrl or anti-miR-59 for 5 days. The percentage of SA-β-gal positive cells was calculated. Scale bars: 100 μm (H). The percentage of the Ki67 positive cells was calculated by immunofluorescence (I). The level of cyclin A2 and lamin B1 was detected by western blot (J).
- K The level of miR-59 was detected in 88- and 92-year-old cells versus 7-year-old cells was assessed by qPCR.
- L 7-year-old cells and 88-year-old cells were transfected with anti-miR-ctrl or anti-miR-59, the level of cyclin A2 and lamin B1 was detected.

Data information: Each experiment was repeated at least three times. Data are presented as the mean ± SD (* $P < 0.05$, ** $P < 0.01$, and *** $P < 0.001$). P -values were calculated by unpaired Student's t -test.

Source data are available online for this figure.

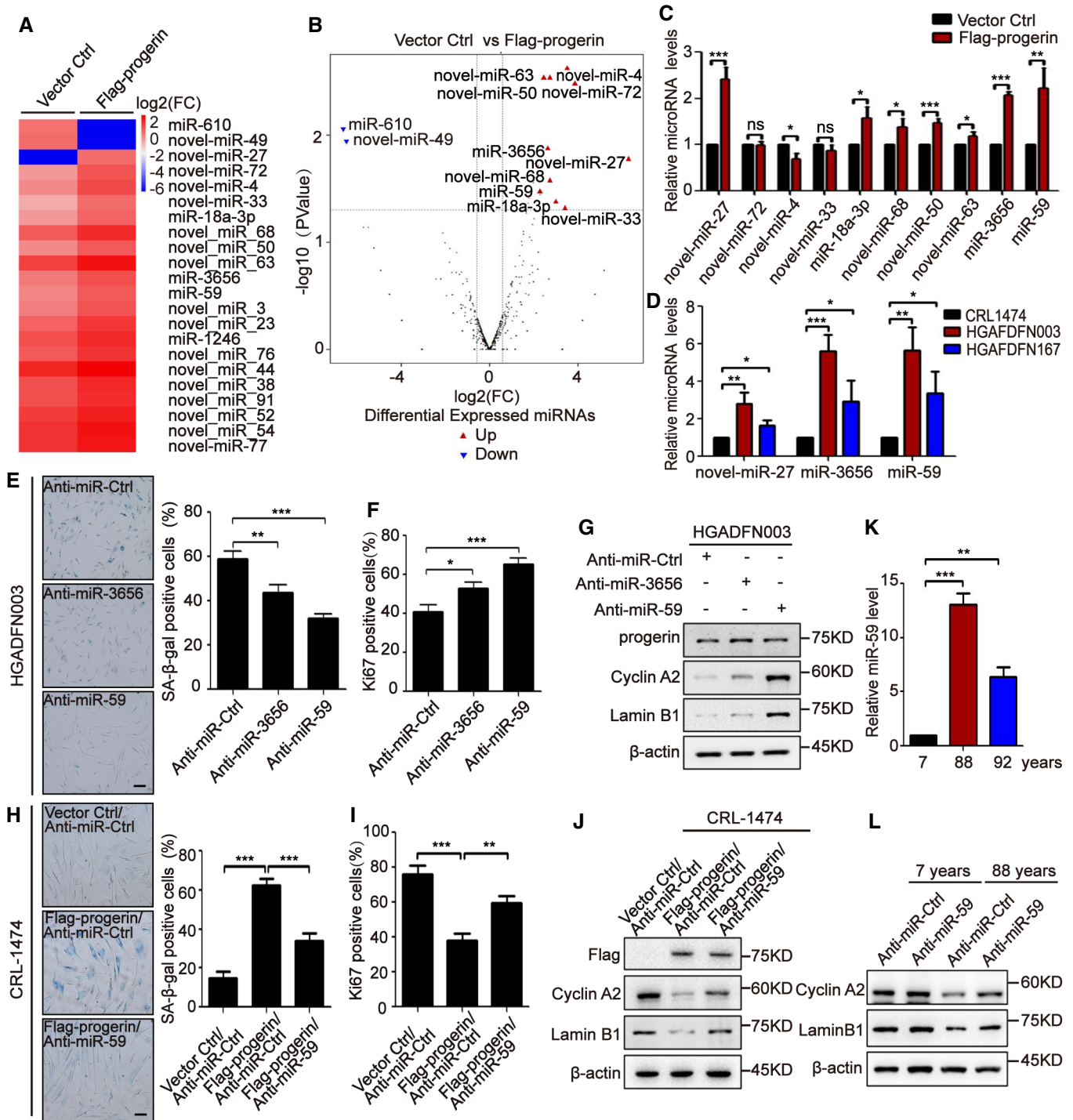


Figure 1.

increased the HMGAs mRNA and protein levels in progerin-expressing CRL-1474 cells (Fig 2D and E). In contrast, overexpression of miR-59 reduced HMGAs gene expression in normal fibroblasts (Fig 2F and G). Consistently, the HMGAs mRNA and protein levels were downregulated in HGPS cells with a high miR-59 level (Figs 2H and I, and EV2A and B). We also showed that the HMGAs mRNA and protein levels were decreased in 88- and 92-year-old cells compared with 7-year-old cells (Fig 2J and K). The expression

of HMGAs was also increased by inhibition of miR-59 in 88-year-old fibroblasts (Fig 2L and M), indicating that miR-59 targeted HMGA genes in HGPS and physiologic senescence.

To test whether the effect of miR-59 on HMGAs was achieved by directly binding to HMGAs 3' UTR, we used TargetScan and miRanda to analyze the binding sites that miR-59 might regulate, followed by luciferase assays. Overexpression of miR-59 was sufficient to decrease the luciferase activity of HMGA1 3'UTR by up to

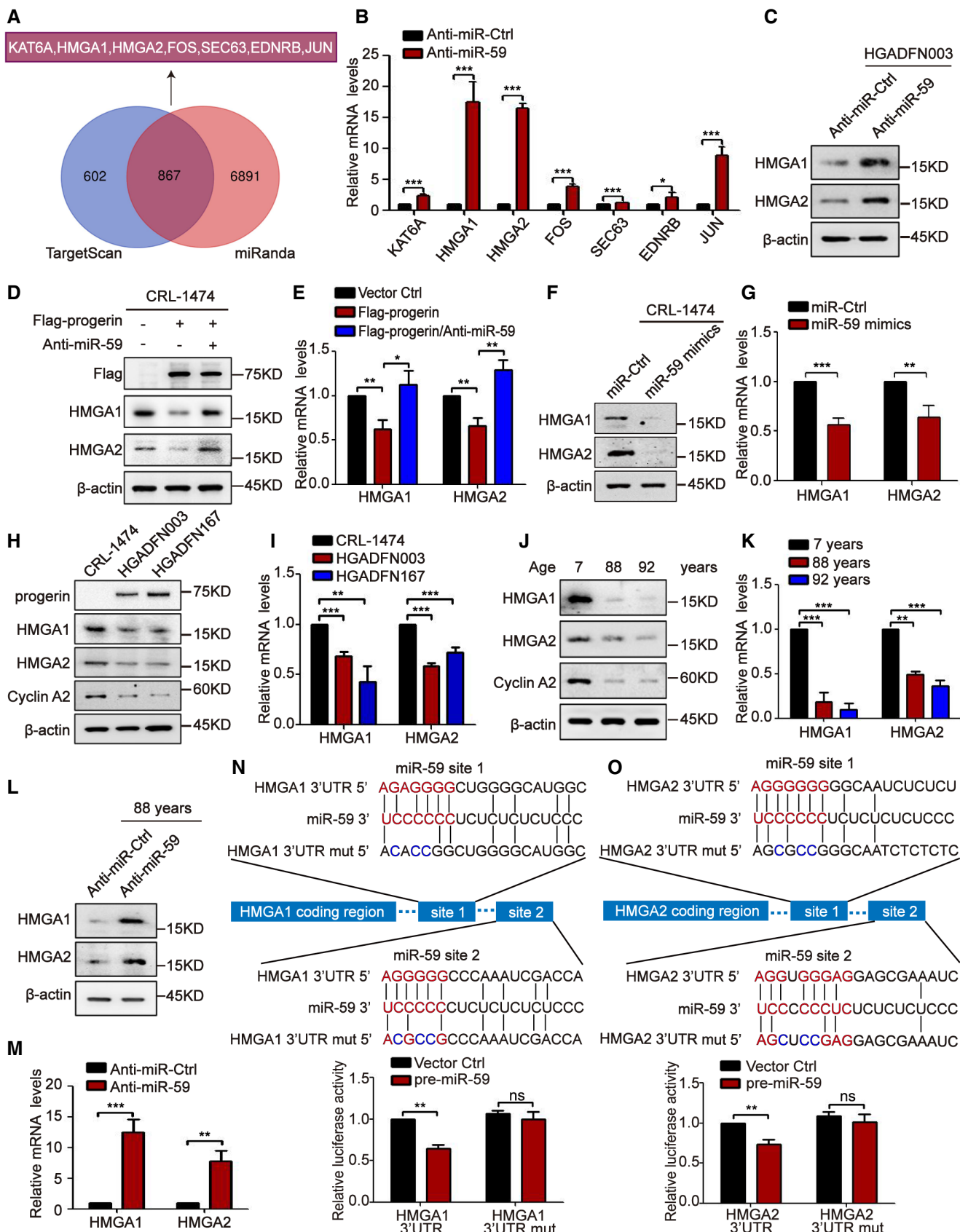


Figure 2.

Figure 2. Screening target genes of miR-59 during HGPS cellular senescence.

- A Venn diagram showing potential target genes of miR-59 predicted by target prediction algorithms (TargetScan and miRanda) and GO analyze of miRNA sequence.
- B, C HGAFDFN003 cells were transfected with anti-miR-ctrl or anti-miR-59 for 5 days, the mRNA level of miR-59-targeting potential genes was assessed by qPCR (B). The protein expression of HMGA1 and HMGA2 was detected by western blot (C).
- D, E After transfection with anti-miR-ctrl or anti-miR-59 in progerin-expressing CRL-1474 cells, the protein expression (D) and mRNA level (E) of HMGA2 were detected.
- F, G Western blot analysis of the expression of HMGA2 (F) and qPCR analysis of the mRNA levels (G) in miR-ctrl or miR-59 mimics-transfected CRL-1474 cells.
- H, I Comparing HGPS patient cells (HGAFDFN003 p22 and HGAFDFN167 p20) with control (CRL-1474 p26), the protein expression (H) and mRNA level (I) of HMGA2 were assessed.
- J, K The protein (J) and mRNA (K) level of HMGA2 were detected in 7, 88 and 92-year-old cells.
- L, M Transfected anti-miR-ctrl or anti-miR-59 in 88-year-old cells, the level of HMGA2 was detected by Western blot (L) and qPCR (M).
- N, O The binding sites of miR-59 on HMGA2 3' UTR were analyzed by TargetScan and miRanda. Luciferase experiments with the wild-type and the mutated 3' UTR of HMGA2 (N)/HMGA1 (O).

Data information: Each experiment was repeated at least three times. Data are presented as the mean \pm SD (* P < 0.05, ** P < 0.01, and *** P < 0.001). P -values were calculated by unpaired Student's t -test.

Source data are available online for this figure.

40%, but when the two binding sites were mutated, no significant effect of miR-59 overexpression was recorded (Fig 2N). Similarly, overexpression of miR-59 reduced the luciferase activity of HMGA2 3'UTR by up to 30%, but when the two binding sites were mutated, no significant effect of miR-59 overexpression was recorded (Fig 2O). Taken together, the results indicated that miR-59 functions as a regulator by directly targeting HMGA genes in HGPS cells.

Anti-miR-59 rescues the HGPS cellular senescence phenotype by upregulating HMGA2

Although HMGA2 are downregulated by miR-59 in HGPS cells, whether HMGA2 have an active role in rescuing impaired cell growth has not been established. To address this issue, a lentiviral transduction system was used to ectopically express Flag-tagged HMGA1 or HMGA2 in HGPS patient fibroblasts. Cell senescence phenotype analyses showed that overexpression of HMGA1 or HMGA2 significantly increased the expression of cyclin A2 and lamin B1 (Fig 3A), reduced the proportion of (SA)- β -gal-positive cells (Fig 3B), and increased Ki67-positive staining cells (Fig 3C). Furthermore, overexpression of HMGA1 or HMGA2 also delayed progerin-expressing CRL-1474 and IMR90 cell senescence (Figs 3D and E, and EV2C–F). In contrast, depletion of HMGA1 or HMGA2 decreased the expression of cyclin A2 and lamin B1 (Fig EV2G and H). Taken together, these data indicated that HMGA1 and HMGA2 have similar roles in alleviating HGPS cellular senescence.

Next, we wondered if the inhibition of miR-59 alleviates cellular senescence by targeting HMGA1 and HMGA2. HGPS patient cells

were transfected with anti-miR-59 and shHMGA2 RNAi lentivirus. Depletion of HMGA2 genes intensified the proportion of (SA)- β -gal-positive cells and reduced Ki67-positive staining cells accompanied with cyclin A2 and lamin B1 downregulation (Fig 3F–H), and anti-miR-59 was still hitting the target genes in the setting of HMGA2 RNAi (Fig EV2I), which confirmed that anti-miR-59 delayed HGPS cell senescence by targeting HMGA1 and HMGA2.

Downregulation of HMGA1 disturbs the interaction between RNAPII and TFIIH during HGPS cellular senescence

The above data provided evidence that both HMGA1 and HMGA2 had roles in ameliorating HGPS cell senescence. This finding led us to determine if HMGA1 and HMGA2 exist in a complex to perform similar functions. Co-IP assays confirmed that HMGA1 and HMGA2 were in the same complex (Figs 4A and B, and EV3A and B). Due to the operability of experiments, we focused on the role and mechanism of action underlying HMGA1 in the following experiment. HMGA1, as a structural protein, binds multiple transcription factors to regulate gene expression (Penzo *et al*, 2019; Teng *et al*, 2019). Therefore, we used the Flag-tagged HMGA1 fusion protein as bait in mass spectrometry to detect the possible regulatory factors. Interestingly, HMGA1 was associated with multiple basal transcription machinery components, including GTF2I, RPABC3, TFIIH4, TFIIH2, and SPT5 (Fig 4C). TFIIH4 and TFIIH2 are two vital subunits of TFIIH, and participate in assembly of the transcription initiation complex (Yan *et al*, 2019). Therefore, we chose TFIIH as a target for more detailed study.

Figure 3. Inhibition of miR-59 alleviates HGPS cellular senescence through targeting HMGA2.

- A–C In Flag-HMGA1 or Flag-HMGA2 infected CRL-1474 and HGPS cells (HGAFDFN003), the level of cyclin A2, lamin B1 was detected by western blot (A). SA- β -gal staining were performed, the percentage of SA- β -gal positive cells was calculated. Scale bars: 100 μ m (B). Expression of Ki67 was analyzed by immunofluorescence. Scale bars: 50 μ m (C).
- D, E Progerin-expressing CRL-1474 cells were transfected with His-control or His-HMGA1. SA- β -gal staining was performed. The percentage of SA- β -gal positive cells was calculated. Scale bars: 100 μ m (D). The level of cyclin A2, lamin B1 was detected by Western blot (E).
- F–H Infection with control shRNA (shCtrl) or HMGA1/HMGA2 shRNA (shHMGA1 and shHMGA2) in anti-miR-59-transfected HGPS cells (HGAFDFN003), cells were subjected to SA- β -gal staining. Scale bars: 100 μ m (F). Cells were subjected to immunofluorescence using anti-Ki67 (red) antibody (left). The percentage of the Ki67 positive cells was calculated. Scale bars: 50 μ m (G). The level of cyclin A2, lamin B1, HMGA1, and HMGA2 was detected by western blot (H).

Data information: Each experiment was repeated at least three times. Data are presented as the mean \pm SD (* P < 0.05, ** P < 0.01, and *** P < 0.001). P -values were calculated by unpaired Student's t -test.

Source data are available online for this figure.

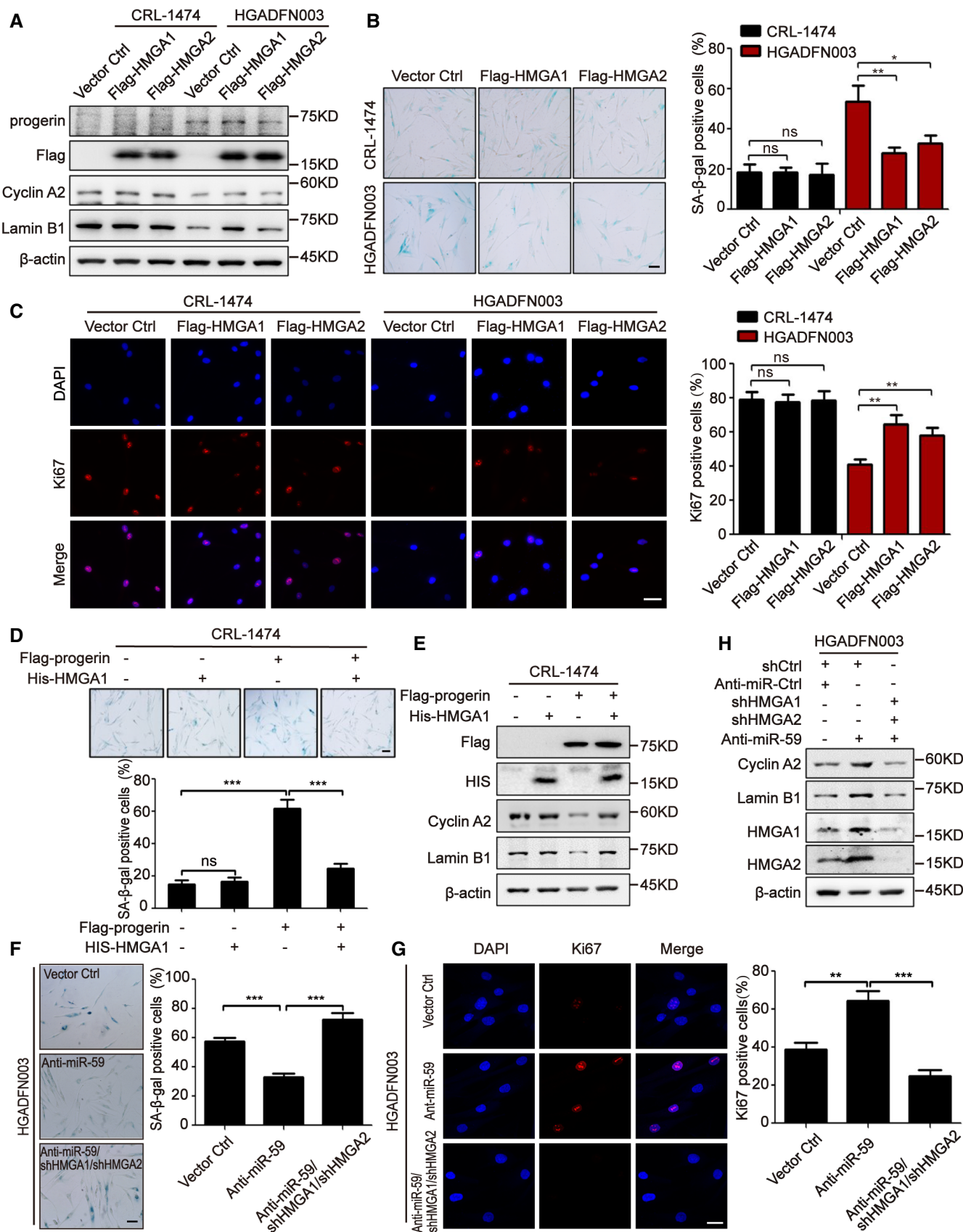


Figure 3.

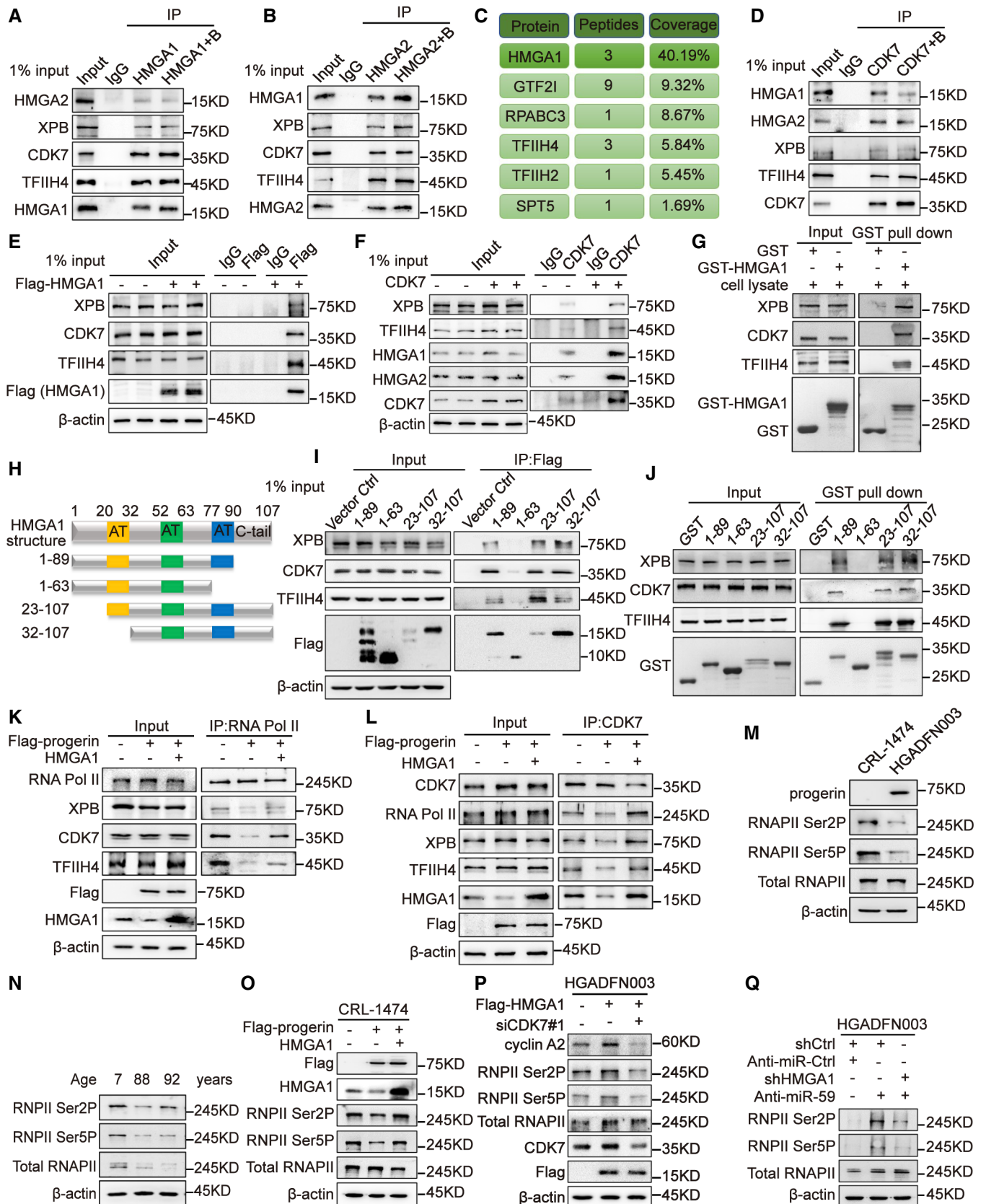


Figure 4.

Figure 4. Analysis of the effect of HMGA1 on the combination of RNAPII and TFIH in HGPS cells.

- A Interaction of endogenous HMGA1 with HMGA2 and TFIH4 complex was analyzed by Co-IP assay using anti-HMGA1 antibody in H1299 cells. Pulled-down protein complexes were analyzed. Benzonase (B) was added in cell lysate.
- B Interaction of endogenous HMGA2 with HMGA1 and TFIH4 complex was analyzed by Co-IP assay using anti-HMGA2 antibody in H1299 cells. Pulled-down protein complexes were analyzed.
- C HMGA1-associated proteins from HEK293T cells expressing FLAG-HMGA1 were IP with anti-Flag antibody. The protein bands were analyzed by mass spectrometry. Representative peptide fragments of HMGA1 associated proteins and peptide coverage of the indicated proteins were shown.
- D Interaction of endogenous CDK7 with HMGA1, XPB and TFIH4 was analyzed by Co-IP assay using anti-CDK7 antibody in H1299 cells. Pulled-down protein complexes were analyzed.
- E-F HEK293T cells were transfected with Flag-HMGA1 (E) or CDK7 (F). HMGA1 or CDK7 was IP with anti-Flag antibody and anti-CDK7 antibody.
- G HEK293T cell lysates were incubated with GST or GST-HMGA1 sepharose beads. Pulled-down protein complexes were analyzed.
- H Scheme of HMGA1 wild-type structure, including AT hooks (AT) and acidic tail (C tail), and deletion mutants used for immunoprecipitation experiments below.
- I HEK293T cells were transfected with Flag-HMGA1 deletion mutants. IP of Flag was performed. Pulled-down protein complexes were analyzed.
- J HEK293T cell lysates were incubated with GST or GST-HMGA1 deletion mutants sepharose beads. Recombinant proteins from pull-down assays visualized by silver staining and Western blot.
- K, L Progerin-expressing H1299 cells were transfected with His-control or His-HMGA1. Immunoprecipitation of RNA Pol II (K) or CDK7 (L) with anti-RNAPII antibody or anti-CDK7 antibody was performed, respectively. Pulled-down protein complexes were analyzed.
- M, N RNAPII, the RNAPII Ser2P, and RNAPII Ser5P in HGAFDFN003 cells (M) and 88, 92-year-old cells (N) compared with CRL-1474 cells were detected by Western blot.
- O Progerin-expressing CRL-1474 cells were transfected with His-control or His-HMGA1. Indicated proteins and modifications were detected by western blot.
- P Infection with siCtrl or siCDK7 in Flag-HMGA1-transfected HGPS cells (HGAFDFN003), cyclin A1, RNAPII, the RNAPII Ser2P and RNAPII Ser5P was detected.
- Q Infection with control shRNA (shCtrl) or HMGA1 shRNA (shHMGA1) in anti-miR-59-transfected HGAFDFN003 cells. Indicated proteins and modifications were detected by western blot.

Source data are available online for this figure.

XPB and CDK7 are two subunits of TFIH with enzymatic activities (Shiekhatter *et al.*, 1995; Kuper & Kisker, 2021). We first verified that HMGA1 and TFIH subunits (TFIIH4, XPB, and CDK7) were in the same complex (Figs 4A and B, D–G, and EV3D and E), and the third AT-hook domain of HMGA1 was responsible for binding with TFIH4, XPB, and CDK7 (Fig 4H–J). Second, we wondered whether downregulation of HMGA1 disturbed the interaction between RNAPII and TFIH in HGPS cells. Co-IP assays using RNA polymerase II (RNAPII) antibody or CDK7 antibody confirmed that downregulation of HMGA1 is accompanied with a reduced combination of TFIH4, XPB, and CDK7 with RNAPII in HGPS cells (Fig 4K and L). Overexpression of HMGA1 in HGPS cells promoted the interaction between RNAPII and TFIH (Fig 4K and L). Like HMGA1, HMGA2, and TFIH subunits, TFIH4, XPB, and CDK7 were also in a same complex, and HMGA2 promoted the combination of TFIH subunits with RNAPII in HGPS cells (Figs 4B and EV3A and C, F–H).

CDK7 mediates phosphorylation of RNAPII serine 5 and 7 (RNAPII Ser5P and Ser7P) during transcription initiation, and RNAPII Ser5P is the initiating form of RNAPII, which represents the transcription initiation process (Akhtar *et al.*, 2009; Glover-Cutter *et al.*, 2009; Chlamydas *et al.*, 2016). Therefore, whether HMGA1 regulates the RNAPII Ser5 phosphorylation level in HGPS cells was determined. First, the RNAPII Ser5P level was significantly decreased in HGPS and senile cells (Figs 4M and N, and EV3I). There was a visible increase of Pol II Ser5P in HMGA1 re-expression HGPS cells (Figs 4O and EV3J and K). HMGA2 also enhanced the RNAPII Ser5P level in HGPS patient cells (Fig EV3J). To confirm the association between HMGA1, CDK7, and RNAPII phosphorylation in HGPS cells, we showed that knocking down of CDK7 decreased RNAPII Ser5 phosphorylation in HMGA1-overexpressed HGPS patient cells, which confirmed that CDK7 played an important role in HMGA1-mediated RNAPII Ser5P in HGPS patient cells (Figs 4P and EV3L). Moreover, we verified HMGA1 alleviated HGPS cellular senescence by CDK7 (Figs 4P and EV3M). In addition, we showed that miR-59 decreased the RNAPII Ser5P level by

targeting HMGA1 in HGPS patient cells (Fig 4Q). We speculated that miR-59 probably regulated transcription initiation by targeting HMGA1.

Re-expression of HMGA1 corrects the abnormal expression of cell cycle genes by activating transcription initiation in HGPS

The above data suggested that HMGA-mediated interaction dysregulation between RNAPII and TFIH might disrupt gene transcription during initiation. First, we performed RNA-seq to reveal which genes were mediated by HMGA1 in progerin-expressing CRL-1474 cells (Fig 5A). The gene expression pattern revealed 1,916 dysregulated genes in HGPS cells compared with control cells, 1,294 genes of which were returned to baseline by re-expression of HMGA1 (Fig 5A and B). These data indicated that HMGA1 had an extensive effect on normalizing gene expression. GO analysis revealed that several pathways were rescued by HMGA1, including those involved in the cell cycle, DNA replication, and the p53 signaling pathway (Figs 5C and EV4A). Among which, 26 cell-cycle-related genes, including CCNA2, CCNB1, and CDK1, exhibited significant downregulation in HGPS and senile cells (Figs 5D and E, and EV4B). Then, genes were returned to baseline while overexpressing HMGA1 or suppressing miR-59 in HGPS patient cells (Figs 5F and G, and EV4B), suggesting that miR-59 regulated the expression of cell cycle genes by targeting HMGA1.

We then wanted to determine if HMGA1 regulated cell cycle genes at gene promoters to initiate gene transcription initiation in HGPS cells. ChIP assays showed increased enrichment of HMGA1 and CDK7 in the cell cycle gene promoters upon re-expression of HMGA1 in HGPS cells (Fig 5H and I). As a phosphorylation substrate for CDK7, the levels of Pol II Ser5P at the HMGA1 target promoters were detected. Similarly, the enrichment of Pol II Ser5P at promoters of HMGA1 targets was upregulated when HMGA1 was overexpressed in HGPS cells (Figs 5J and EV4C and D). These data established that HMGA1 is required for efficient phosphorylation of Pol II Ser5 at the target genes.

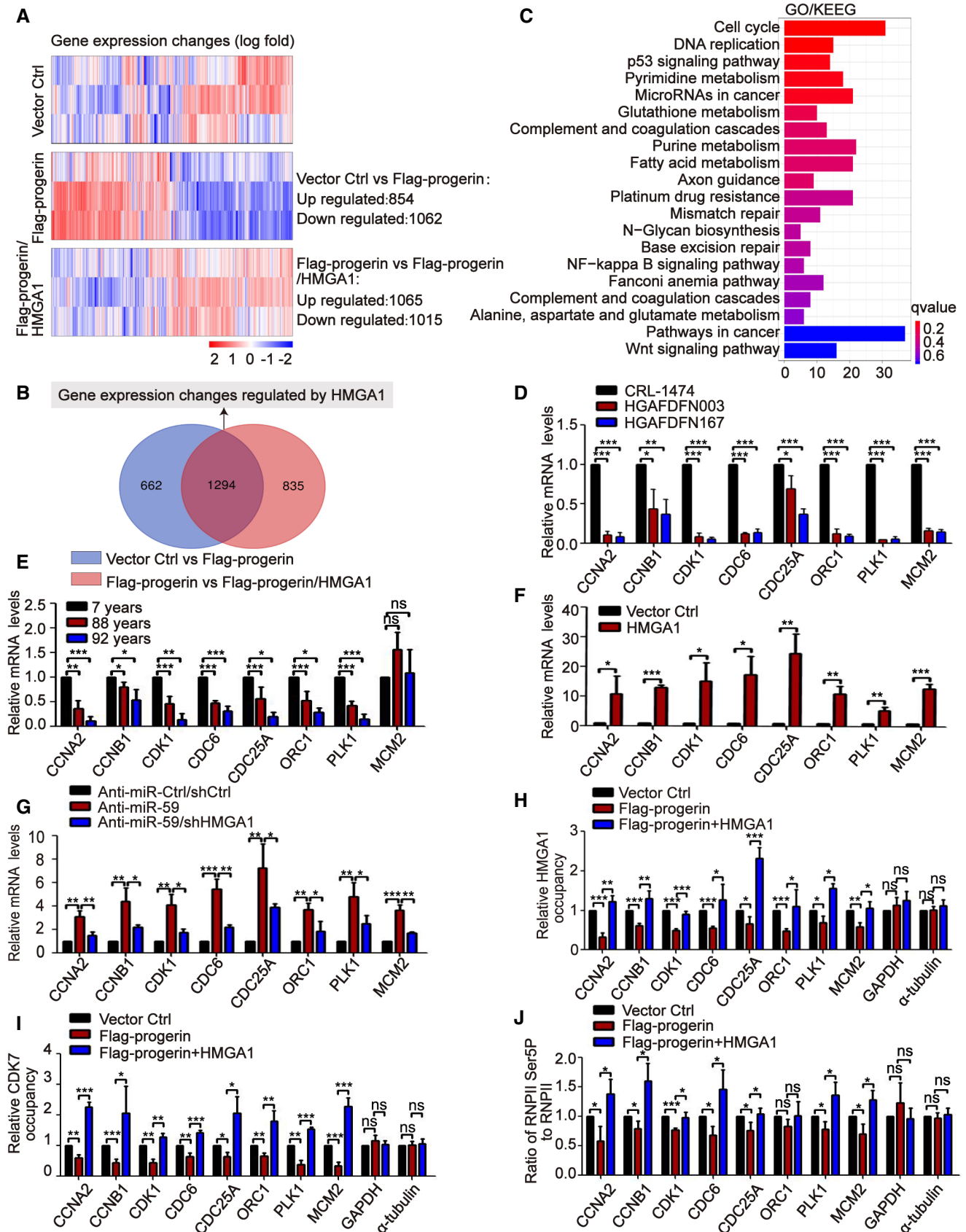


Figure 5.

Figure 5. The role of HMGA1 on regulating expression of the cell cycle genes in HGPS.

A–C Progerin-expressing CRL-1474 cells were transfected with His-control or His-HMGA1. Heatmap showing differential gene expression as determined by RNA-seq in HGPS cells, $P < 0.05$. Lowly expressed genes are shown in blue, highly expressed ones in red (A). Venn diagram showing the number of overlapping genes between HGPS cells versus control cells and His-HMGA1-transfected HGPS cells versus His-control-transfected HGPS cells (B). GO enrichment analysis of HMGA1-regulated genes (C).

D, E The mRNA level of cell cycle genes in HGPS patient cells (HGAFDFN003 and HGAFDFN167) (D) and 88- and 92-year-old cells (E) was assessed by qPCR.

F HGAFDFN003 cells were infected with His-HMGA1 and the mRNA level of cell cycle genes was assessed by qPCR.

G Infection with control shRNA (shCtrl) or HMGA1 shRNA (shHMGA1) in anti-miR-59-transfected HGAFDFN003 cells. The mRNA level of cell cycle genes was assessed by qPCR.

H–J Progerin-expressing CRL-1474 cells were transfected with His-control or His-HMGA1. CHIP–qPCR analyses for HMGA1 (H), CDK7 (I), ratio of RNAPII Ser5P/RNAPII (J).

Data information: Each experiment was repeated at least three times. Data are presented as the mean \pm SD (* $P < 0.05$, ** $P < 0.01$, and *** $P < 0.001$). P -values were calculated by unpaired Student's t -test.

Anti-miR-59 therapy ameliorates the phenotype and extends longevity in *Lmna*^{G609G/G609G} mice

To evaluate the therapeutic potential of anti-miR-59 *in vivo*, we successfully generated an *Lmna*^{G609G/G609G} mouse model (ICR background) using the BE4-Gam gene editing system (Fig EV5A–E). In agreement with the HGPS cell findings, the miR-59 level was increased in multiple tissues of *Lmna*^{G609G/G609G} mice, such as the heart, liver, lung, kidney, skin, and muscle, compared with wild-type mice (Fig 6A). Conversely, the Hmgas mRNA level was decreased in the tissues of *Lmna*^{G609G/G609G} mice (Fig 6B and C). We needed to confirm if miR-59, as a new-found miRNA in human HGPS cell senescence, also targeted Hmgas in mice (Fig 6D). TargetScan and miRanda projected that the binding sites of miR-59 on Hmgas 3' UTR in mice were highly similar to humans (Fig 6E and F). Luciferase assays confirmed that miR-59 directly targeted murine Hmgas 3' UTR (Fig 6G and H). Next, we chose an adeno-associated virus 9 (AAV9) delivery vector, taking advantage of its safety and broad tissue tropism to assess the efficacy of anti-miR-59 *in vivo*. Given that HGPS is a pediatric systemic disease, we systemically delivered the AAV9-mCherry-anti-miR-59 into mice via an intraperitoneal injection. mCherry reporter was detectable on day 30 post-injection in multiple organs, including the skin, heart, muscle, aorta, vertebrae, kidney, legs, and lung (Figs 7A and B, and EV6A and B).

After treatment with AAV9-anti-miR-59, the mice at the same age had a healthier appearance, with improved posture, retarded loss of grooming, and less kyphosis (Figs 7C and D, and EV6C; Movie EV1) compared with untreated mice. The weight of HGPS mice gradually decreased with age (Osorio *et al*, 2011). We monitored the body weight progression from 4-week-old mice and observed that treatment with AAV9-anti-miR-59 attenuated weight loss in HGPS mice (Figs 7E–H). Importantly, the median survival rate increased by approximately 25.5%. The median survival rates for untreated and treated mice with HGPS were 98 and 123 days, respectively. The mean survival was extended from 99.5 days (SD 9.09) to 123.4 days (SD 10.68; Figs 7I and EV6D and E).

The musculoskeletal system is one of the major systems impaired during HGPS premature aging, seriously affecting the quality of life (Beyret *et al*, 2019). We measured the voluntary activity by open field experiments, which was enhanced in treated mice compared with untreated (Figs 8A and EV6F). This finding can be interpreted as reduced perivascular fibrosis in quadriceps muscle (Fig 8B). Moreover, we analyzed the aorta and heart fibrosis in HGPS mice because HGPS patients mainly die from cardiovascular ailments. The treatment decreased the adventitial thickness of the aorta and

perivascular fibrosis in heart compared with control mice (Fig 8B and C). The treatment also suppressed epidermal thinning and dermal fat loss, two aging-associated skin conditions (Fig 8D). To substantiate whether anti-miR-59 increased Hmgas in HGPS mice, we detected miR-59 level and the target genes of miR-59, Hmgas mRNA level. The results showed miR-59 level had no significant changes (Fig 8E), but increased Hmgas mRNA level in multiple tissues from anti-miR-59-transduced mice compared with control (Fig 8F and G). Consistently, immunohistochemical analysis showed that there was a significant enhancement in Hmgas-positive nuclei in the skin, heart, lung, and muscle from anti-miR-59-transduced mice compared with control (Figs 8H and EV6G–I). Furthermore, progerin levels did not decrease significantly in the heart, lung, skin, and muscle of anti-miR-59-treated HGPS mice compared with untreated ones (Fig EV6J), which indicated that miR-59 had little effect on progerin expression. Taken together, delivery of AAV9-anti-miR-59 in *Lmna*^{G609G/G609G} mice ameliorated the aging phenotype and extended longevity.

Discussion

In this study, we discovered a novel miRNA (miR-59) in HGPS cells. Inhibition of miR-59 alleviated the premature senescence phenotype in HGPS cells, ameliorated the premature aging phenotype, and extended longevity in *Lmna*^{G609G/G609G} mice. Moreover, we unveiled a novel regulatory mechanism of miR-59-regulated expression of cell cycle genes by regulating HMGA1 and HMGA2. We propose a model in which progerin leads to augmentation of miR-59, which downregulates HMGA2 through post-transcriptional inhibition. Anti-miR-59 increased the combination of TFIIH and RNAPII by upregulating HMGA1 and HMGA2, then activated transcription initiation of cell cycle genes by increasing enrichment RNAPII Ser5 on chromatin, and ultimately ameliorated HGPS cell senescence (Fig 9).

miRNAs have become useful tools and targets for novel therapeutic approaches in multiple diseases, we are wondering if we could develop new therapeutic techniques for HGPS through targeting miRNAs. Therefore, we focused on miRNAs and identified the role of miR-59 during HGPS senescence. Then we intended to explore the mechanism of miR-59 in HGPS therapy and focused on putative upregulated miRNA targets in anti-miR-59-transfected HGPS patient cells. Furthermore, many genes have been reported to be downregulated during HGPS cellular senescence, such as LAP2 α , LaminB1, HP1 α , EZH2, and Sirt7. Our previous study also showed that some significant genes related to senescence were

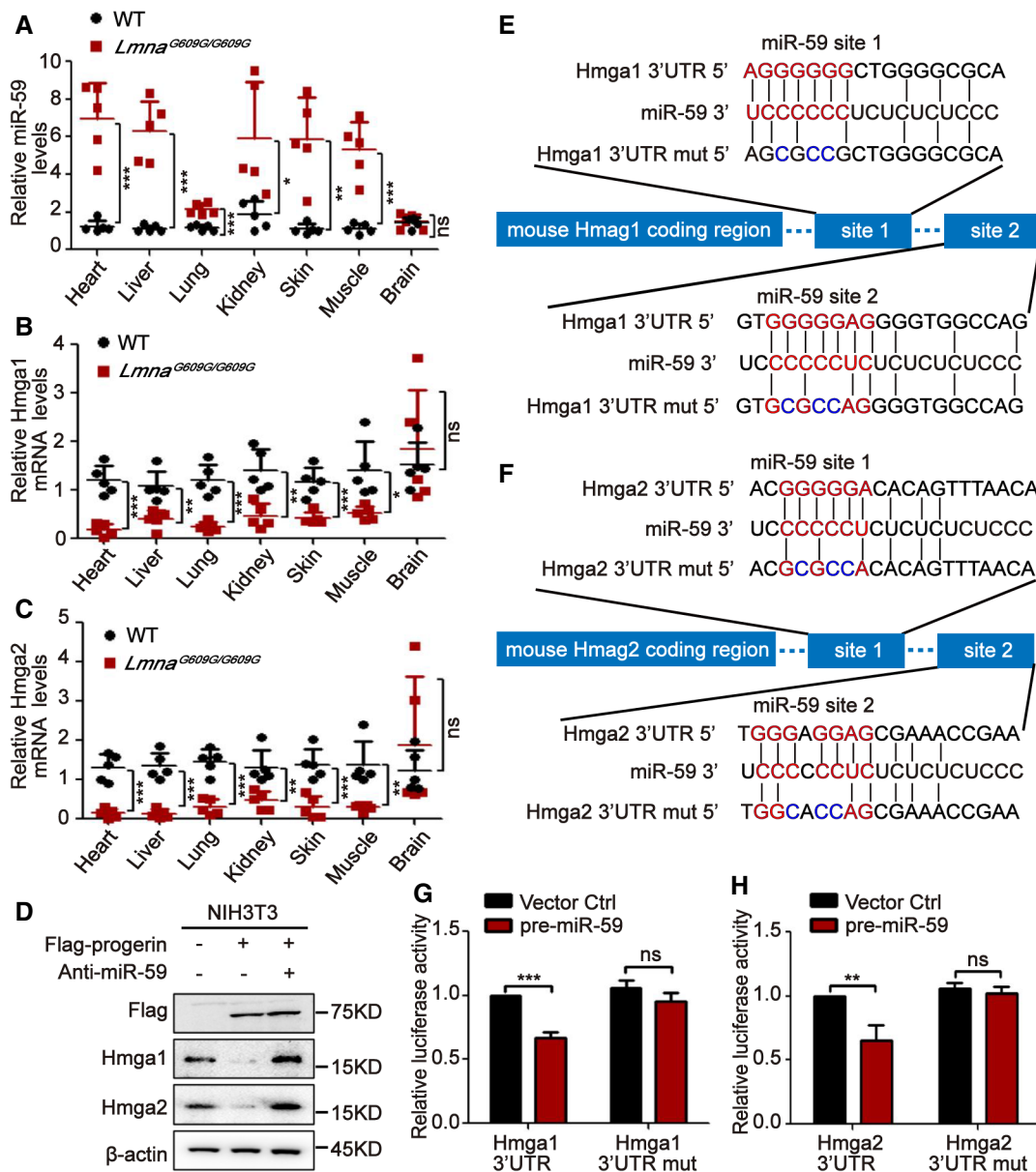


Figure 6. Hmga1 and Hmga2 are target genes of miR-59 in mice.

A miR-59 was detected in heart, liver, lung, kidney, skin, muscle, and brain of *Lmna*^{G609G/G609G} mice by qPCR at 12 weeks of life ($n = 5$ for each group).

B, C The mRNA level of Hmga1 (B) and Hmga2 (C) was detected in the heart, liver, lung, kidney, skin, muscle and brain of *Lmna*^{G609G/G609G} mice by qPCR at 12 weeks of life ($n = 5$ for each group).

D Transfected anti-miR-Ctrl or anti-miR-59 in progerin-expressing NIH3T3 cells. Western blot analysis of HMGAs.

E, F The binding sites of miR-59 on mice Hmga 3' UTR were analyzed.

G, H Luciferase experiments with the wild-type and the mutated 3' UTR of Hmga1 and Hmga2.

Data information: Each experiment was repeated at least three times. Data are presented as the mean \pm SD ($*P < 0.05$, $**P < 0.01$, and $***P < 0.001$). P -values were calculated by unpaired Student's t -test.

Source data are available online for this figure.

downregulated after overexpressing progerin. Therefore, we focused on the miRNAs that were upregulated after overexpressing progerin. We also planned to investigate the role of the downregulated miRNAs in HGPS in the near future.

Previous reports have shown that miR-9 is a brain-specific miRNA and progerin mRNA is a target of miR-9, which allows miR-9

to prevent progerin accumulation in HGPS brain (Jung *et al.*, 2012; Nissan *et al.*, 2012), leading to relatively normal brains in HGPS patients. These studies also explained why miR-59 had no evident change in the brains of HGPS mice compared with normal mice. Without the protection of miR-9 in other tissues, however, progerin was overexpressed (Fig EV5D). Thus, miR-59 was upregulated by

progerin in other tissues except the brain (Fig 6A). Similarly, Hmga5 had a significant negative correlation with miR-59 in relative tissues (Fig 6B and C). Actually, the intraperitoneal injection of AAV9-mCherry-anti-miR-59 was distributed in a variety of tissues including the skin, heart, muscle, vertebrae, kidneys, and legs, although some tissues exhibited the low level of a mCherry signal, such as the brain (Figs 7B and EV6A and B). Because the level of miR-59 was not upregulated in HGPS mice brain, we considered that the injection protocol was still effective for the systemic treatment of HGPS mice.

Previous studies have shown that HMGAs have different roles in cell senescence models (Narita *et al*, 2006; Nishino *et al*, 2008; Yu *et al*, 2013). HMGA1 and HMGA2 are increased in oncogenic RAS-induced cell senescence; knockdown of HMGA1 alleviates senescence phenotypes (Narita *et al*, 2006). In contrast, in human umbilical cord blood-derived stromal cells (hUCBSCs), HMGA2 is downregulated as the number of cell passage increases, resulting in upregulation of p16 and p21, thus indicating that decreased HMGA2 promotes hUCBSC senescence (Yu *et al*, 2013). HMGA2, as a

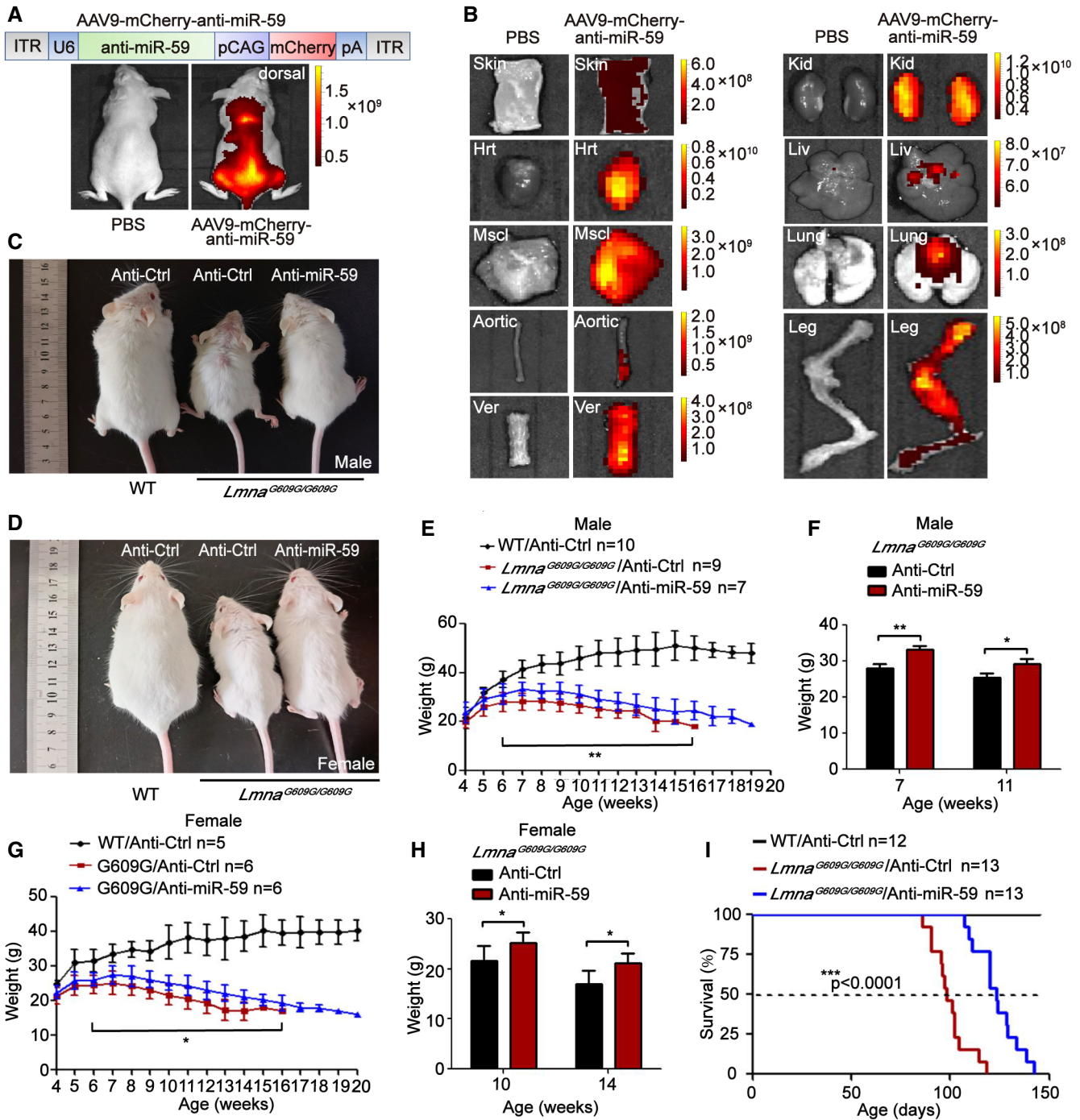


Figure 7.

Figure 7. Delivery of anti-miR-59 prolongs lifespan in *Lmna*^{G609G/G609G} mice.

- A The *in vivo* therapy scheme. Eight-day-old mice were injected intraperitoneally with AAV9-mCherry-anti-miR-59 (5×10^{11} viral particles). The mCherry signals were detected 30 days post-injection (DPI) in *Lmna*^{G609G/G609G} mice versus PBS-injected control (dorsal).
- B Expression of the mCherry reporter in different organs at 30DPI in *Lmna*^{G609G/G609G} mice versus PBS-injected control. Hrt, MscI, Ver, Kid, Liv: heart, muscle, vertebrae, kidney, liver. AAV9-mCherry-anti-miR-59 was injected into 8-day-old mice and detected at different points.
- C, D The gross morphology of the wild-type and *Lmna*^{G609G/G609G} mice injected with anti-ctrl or anti-miR-59 for 14 weeks.
- E Progression of body weight of male mice transduced with anti-Ctrl versus anti-miR-59 was detected from 4 weeks of life. The sample size (*n*) indicates the initial number of mice at week 4, initial *n* = 10 WT; *n* = 9 anti-Ctrl-transduced mice; *n* = 7 anti-miR-59-transduced mice. Shown are mean values \pm standard deviations, two-sided *t*-test was used when comparing anti-Ctrl-transduced mice and anti-miR-59-transduced mice from week 6 to 16.
- F Body weight comparison at 7- and 11-week-old male mice (*n* = 9 anti-Ctrl-transduced mice; *n* = 7 anti-miR-59-transduced mice). Data are presented as the mean \pm SD (**P* < 0.05, ***P* < 0.01). *P*-values were calculated by unpaired Student's *t*-test.
- G Progression of body weight of female mice transduced with anti-Ctrl versus anti-miR-59 was detected from 4 weeks of life. The sample size (*n*) indicates the initial number of mice at week 4, initial *n* = 5 WT; *n* = 6 anti-Ctrl-transduced mice; *n* = 6 anti-miR-59-transduced mice. Shown are mean values \pm standard deviations, two-sided *t*-test was used when comparing anti-Ctrl-transduced mice and anti-miR-59-transduced mice from week 6 to 16.
- H Body weight comparison at 7- and 11-week-old female mice (*n* = 6 for each group). Data are presented as the mean \pm SD (**P* < 0.05). *P*-values were calculated by unpaired Student's *t*-test.
- I Kaplan–Meier survival plot of the wild-type and *Lmna*^{G609G/G609G} mice which injected with anti-Ctrl or anti-miR-59 (*n* = 12 WT; *n* = 13 anti-Ctrl-transduced mice; *n* = 13 anti-miR-59-transduced mice, two-sided log-rank test).

Source data are available online for this figure.

transcriptional regulator, is highly expressed in fetal neural stem cells (NSCs) of mice, but the expression declines with age. HMGA2 promotes fetal and young-adult stem cell self-renewal by decreasing p16(Ink4a)/p19(Arf) expression (Nishino *et al*, 2008). In the current study, we found that HMGA1 and HMGA2 had similar active roles in rescuing HGPS and physiologic cell senescence for the first time, which is consistent with the function of HMGA2 in hUCBSCs and NSCs. We wondered why HMGAs, as vital chromatin-regulated proteins, have an opposing role in multiple cell senescence models. In fact, oncogenic RAS-induced cell senescence is accompanied by the formation of senescence-associated heterochromatic foci (SAHF). SAHF formation was decreased by knockdown of HMGA1 (Narita *et al*, 2006). In contrast to RAS-induced cell senescence, however, the heterochromatin is less in HGPS and physiologic senescence cells than in normal cells. It remains to be studied whether the loss of heterochromatin is mediated by HMGAs. Therefore, according to the state of heterochromatin, we concluded that acute cell senescence is accompanied by the formation of SAHF and increased HMGAs. HMGAs are decreased during chronic cell senescence accompanied by the loss of heterochromatin, such as HGPS and physiologic cellular senescence.

Our results showed that HMGA1 is required for efficient phosphorylation of Pol II Ser5 at the gene promoter to activate cell cycle gene transcription initiation. In addition, phosphorylation of Pol II Ser2 was regulated by HMGA1 in whole HGPS cell lysates, indicating that overexpression of HMGA1 might activate the transcription

elongation process (Figs 40 and EV3J). It has been reported that inhibition of Kin28/CDK7 blocks phosphorylation of RNA Pol II Ser5 and RNA Pol II Ser2 *in vitro*, then reduces elongation efficiency (Joo *et al*, 2019). Whether HMGA1 increases the enrichment of CDK7 on the gene by promoting assembly of the basal transcriptional machinery, thus enhancing elongation efficiency warrants further study. Moreover, a previous study revealed that in the transcription process of HIV, 7SK regulated the combination of HMGA1 and the transcription elongation factor (P-TEFB) in the core promoter region of HIV, thus inhibiting the transcription elongation of HIV (Eilebrecht *et al*, 2011). Based on mass spectrometry, transcription elongation factors, such as SPT5, also interact with HMGA1 (Fig 4C). Whether HMGA1 improves transcription elongation by increasing binding to the transcription elongation factor in HGPS cells warrants further study.

As reported, *Hmga1*-KO mice have cardiac diseases and type 2 diabetes, while *Hmga2*-KO exhibits a pygmy phenotype (Foti *et al*, 2005). The KO phenotype is not consistent with HGPS mice. Our results indicated that downregulation of HMGA1 and HMGA2 facilitates the HGPS phenotype. Based on our results and previous reports, many genes are regulated by HMGA proteins (Narita *et al*, 2006; Sgarra *et al*, 2018; Vignali & Marracci, 2020; Sharma *et al*, 2022). It is apparent that several functions exerted by one member of the HMGA family are, at least partially, compensated by the other family member. Therefore, if one of the HMGA family proteins is knocked out alone, the other protein might exert a

Figure 8. Anti-miR-59 therapy ameliorates aging phenotype in *Lmna*^{G609G/G609G} mice.

AAV9-mCherry-anti-miR-59 was injected into 8-day-old mice and detected at different points.

- A Running ability of male mice transduced with anti-Ctrl versus anti-miR-59 at 12 weeks of life (*n* = 5 for each group).
- B, C Masson staining showed the perivascular interstitial fibrosis in the heart and quadriceps muscle (B) (Scale bars, 50 μ m), the adventitial fibrosis (blue areas), and the adventitial width of aorta (C). The boxes and arrows denoted the aortic adventitia. Scale bars, 200 μ m (top), 50 μ m (lower).
- D H&E staining in skin showed the epidermis and fat layer of skin. Scale bars, 150 μ m. The boxes and arrows denoted epidermis and vertical bars indicated fat layer.
- E The level of miR-59 was detected in the heart, liver, lung, kidney, skin, and muscle of *Lmna*^{G609G/G609G} mice (*n* = 5 for each group).
- F, G The mRNA level of *Hmga1* (F) and *Hmga2* (G) was detected in the heart, liver, lung, kidney, skin, and muscle of *Lmna*^{G609G/G609G} mice (*n* = 5 for each group).
- H *Hmga*s immunohistochemistry in skin of WT mice and *Lmna*^{G609G/G609G} mice. Scale bars, 50 μ m.

Data information: Masson staining, H&E staining and immunohistochemistry were shown at 14 weeks of life, *n* = 5 for each group. Each experiment was repeated at least three times. Data are presented as the mean \pm SD (**P* < 0.05, ***P* < 0.01, and ****P* < 0.001). *P*-values were calculated by unpaired Student's *t*-test.

Source data are available online for this figure.

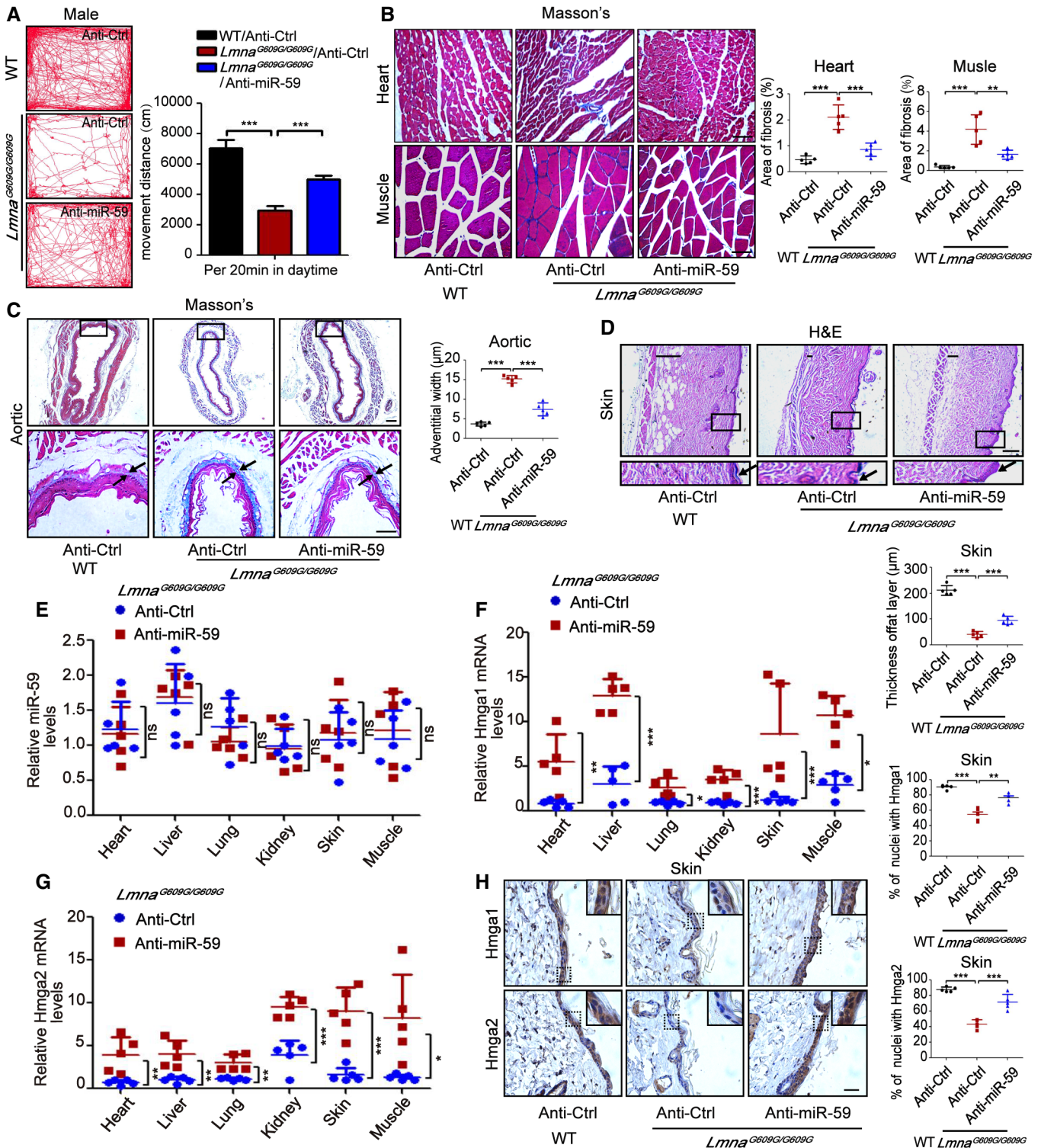


Figure 8.

compensating role, which explains why the mice KO model of Hmga1 or Hmga2 alone did not exhibit a very severe HGPS phenotype. Other than HMGA1 and HMGA2, progerin also caused multiple proteins that had roles in HGPS cellular senescence to change. Our results verified, to a large extent, that inhibition of miR-59

ameliorated premature aging phenotype and extended longevity in *Lmna*^{G609G/G609G} mice by targeting both Hmga1 and Hmga2.

The aging pattern of HGPS resembles normal aging, suggesting that HGPS is an accelerated version of physiologic aging. The features of HGPS represent a paradigm for translational medicine in the area of

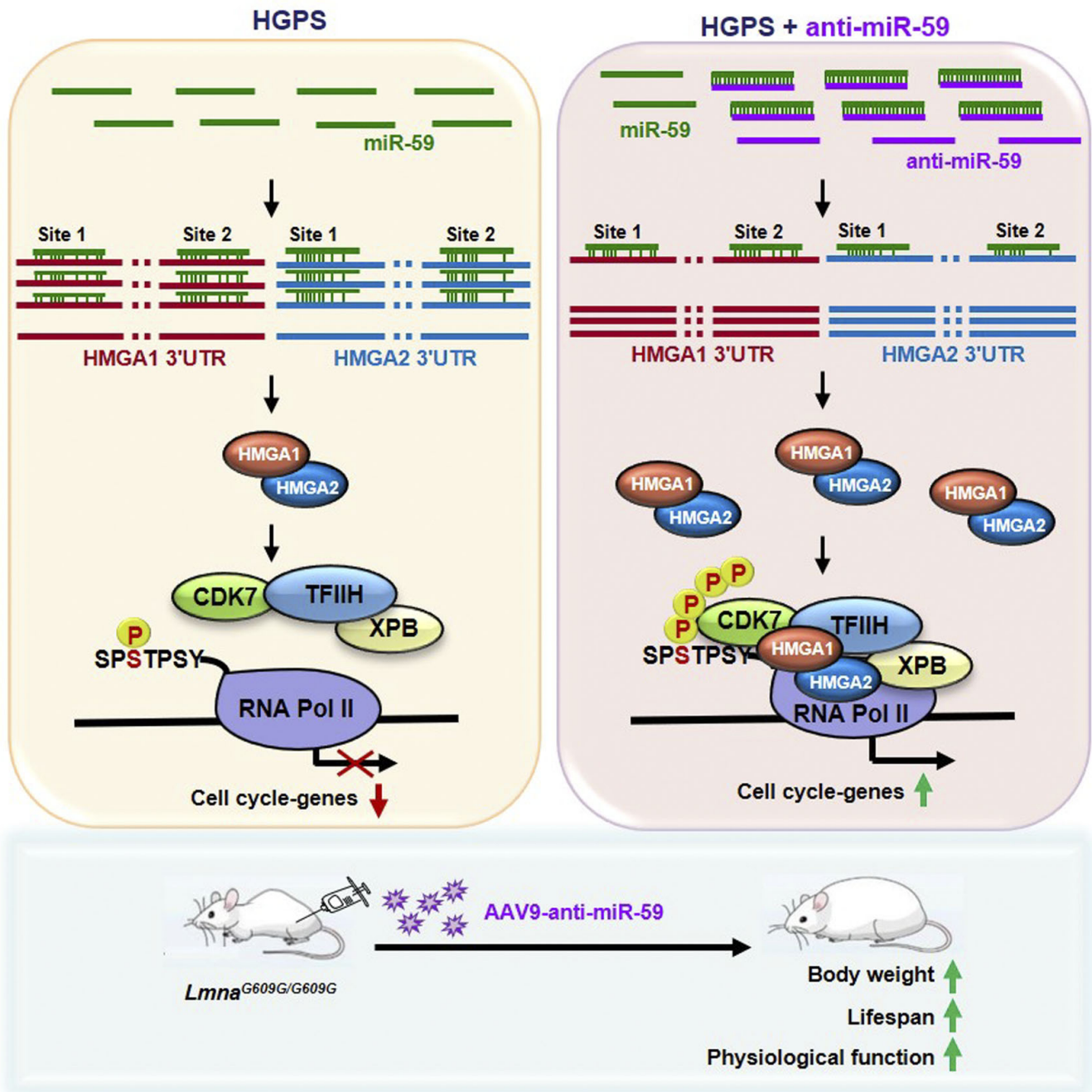


Figure 9. A proposed model for anti-miR-59 in alleviating HGPS cellular.

Progerin led to the augmentation of miR-59, which downregulated HMGAs, HMGAs, further disturbed the combination of RNAPII and TFIIH, resulting in abnormal expression of cell cycle genes in HGPS cells. Inhibition of miR-59 upregulated HMGAs, thereby facilitated interaction between RNAPII and TFIIH, further activated the transcription initiation of the cell cycle genes by increasing enrichment of RNAPII Ser5 on chromatin, ultimately ameliorated HGPS cell senescence. *In vivo*, inhibition of miR-59 ameliorated premature aging phenotype and extended longevity in *Lmna*^{G609G/G609G} mice.

aging research (Gordon *et al*, 2014b; Cenni *et al*, 2020). In our study, we observed that miR-59 inhibition alleviated the senescence of cells, which were derived from an 88-year-old individual (Figs 1L and EV1G–J), which hinted to us that anti-miR-59 has the potential for treatment in physiologic aging. Therefore, in corollary studies, we plan to deliver AAV9-anti-miR-59 in physiologically aged mice to explore

the possibility of miR-59 as a drug target in improving physiologic aging. Therapeutic approaches include FTIs, and autophagy activation with rapamycin analogs has side effects (Cao *et al*, 2011; Dhillon, 2021). Whether the treatment of anti-miR-59 in *Lmna*^{G609G/G609G} mice will have side effects, such as liver and kidney injury, and drug toxicity, needs to be verified in additional experiments.

To date, preclinical and clinical successes in AAV-mediated gene replacement, gene silencing, and gene editing have helped AAV gain popularity as the ideal therapeutic vector. Indeed, two AAV-based therapeutics have been approved for use in Europe and the United States (Wang *et al*, 2019). Moreover, it has been reported that miRNA interventions based on AAV9 were performed. Specifically, AAV9-induced overexpression of miR-17 in skeletal muscle ameliorated whole-body insulin resistance in di(2-ethylhexyl) phthalate (DEHP)-exposed mice (Wei *et al*, 2020). In addition to an AAV9-mediated miRNA delivery system, there are other delivery methods for miRNA therapeutics, including poly (lactide-co-glycolide [PLGA]), neutral lipid emulsions (NLEs), nanoparticles, polyethylenimine (PEI), and N-acetyl-D-galactosamine [GalNAc] (Rupaimoole & Slack, 2017). For example, anti-miRNAs can be conjugated to GalNAc, which leads to uptake in cells by clathrin-mediated endocytosis. GalNAc is currently being evaluated in phase I and II trials (Rupaimoole & Slack, 2017). Anti-miR-155 is delivered by an LNA-modified antisense inhibitor to treat cutaneous T cell lymphoma and mycosis fungoides, which is being evaluated in phase I trials (Babar *et al*, 2012). We intend to evaluate the efficacy of these delivery systems compared with AAV9-mediated anti-miR-59 to provide a basis for evaluation of preclinical treatment of HGPS.

Materials and Methods

Cell cultures and treatment

CRL-1474, IMR90, HEK293T, H1299, and NIH3T3 cells were obtained from the American Type Culture Collection (ATCC). HGAFDFN003 and HGAFDFN167 cells were obtained from The Progeria Research Foundation (PRF). AG05247 (88-years-old) and AG09602 cells (92-years-old) were obtained from the Coriell Cell Repository (CCR). Cells were cultured in Dulbecco's modified Eagle's medium (DMEM) supplemented with 10% fetal bovine serum (VivaCell) (HGPS patient and senile cells were supplemented with 15% fetal bovine serum), and penicillin–streptomycin. CRL-1474, IMR90, HGAFDFN003, HGAFDFN167, AG05247, and AG09602 were cultured at 37°C in 5% CO₂ and 5% O₂. HEK293T, H1299, and NIH3T3 cells were cultured at 37°C in 5% CO₂. Cells were tested by a MycoBlue Mycoplasma Detector (Vazyme Biotech, Nanjing, China) to exclude *Mycoplasma* contamination before experiments. miR-59 mimics, antagonist anti-miR-59, and anti-miR-3656 were purchased from Gemma Biology (Shanghai, China).

AntimiRs, miRNA mimics, and pre-miRNA sequence

Anti-miR-59 sequence: 5'-AGGGGGGAGAGAGAGAGGG-3'
 Anti-miR-3656 sequence: 5'-CCACCCCGCACCCGCC-3'
 miR-59 mimics' sequence: 5'-CCUCUCUCUCUCCCCCU-3'
 pre-miR-59 sequence: 5'-AGAUUUAGACGAAGGGAGAGAGAUGGC
 GGG AGAAGCCACACCCUCACACACUCACACACGCUCAUACTC
 CCUCUCUCUCUCCCCCUCCUCUCUCUCUCAUACA-3'

RNA and miRNA extraction, RT-PCR, and real-time PCR analysis

Total RNA was extracted from cells using Trizol reagent (Takara, Dalian, China) following the manufacturer's instructions. The cDNA was synthesized with the Reverse Transcription System (Promega).

Real-time PCR was carried out on an QuantStudio™ 3 Realtime-PCR Instrument (ABI, Singapore) using SYBR Green Real-time PCR Master Mix (Takala). β-actin was used as an internal control. The primer sequences for PCR, which were synthesized by Comate Bioscience (Changchun, China), were as follows:

β-actin_fwd (5'-GAGCACAGAGCCTCGCCTT-3')
 β-actin_rev (5'-ATCCTTCTGACCCATGCCA-3')
 HMGA1_fwd (5'-AGCGAAGTGCCAACACCTAAG-3')
 HMGA1_rev (5'-TGGTGGTTTCCGGGTCTTG-3')
 HMGA2_fwd (5'-ACCCAGGGGAAGACCCAAA-3')
 HMGA2_rev (5'-CCTCTTGGCCGTTTTTCTCCA-3')
 CCNA2_fwd (5'-TTCATTTAGCACTCTACACAGTCACGG-3')
 CCNA2_rev (5'-TTGAGGTAGTCTGGTGAAGTCC-3')
 CCNB1_fwd (5'-TGGAAAAGTTGGCTCCAAAG-3')
 CCNB1_rev (5'-TCAGAAAAGCTTGGCAGAGA-3')
 CDK1_fwd (5'-CCCTTTAGCGCGGATCTACC-3')
 CDK1_rev (5'-CATGGCTACCACTGACCTGT-3')
 CDC6_fwd (5'-TGTTCTCTCGTGTAAAAGCC-3')
 CDC6_rev (5'-GAATGGCAGGCTTGGTGTG-3')
 CDC25A_fwd (5'-ACCGTCACTATGGACCAGC-3')
 CDC25A_rev (5'-TTCAGAGCTGGACTACATCC-3')
 ORC1_fwd (5'-CGATTGGCGGAAGTTTTCT-3')
 ORC1_rev (5'-CTTGTGGGGTAGTGTGCCAT-3')
 PLK1_fwd (5'-CGTGACCTACATCGACGAGA-3')
 PLK1_rev (5'-GGAGGGCAGCTATTAGGAGG-3')
 MCM2_fwd (5'-TGTCACCTGCTCTGCCACTAA-3')
 MCM2_rev (5'-GCAGCATGCGCAAGACTTT-3')
 KAT6A_fwd (5'-CAGTGGCCATCCATCCTGTT-3')
 KAT6A_rev (5'-TCGACAGGAGTGCATTT-3')
 FOS_fwd (5'-CAGACTACGAGGCGTCATCC-3')
 FOS_rev (5'-TCTGCGGGTGAGTGGTAGTA-3')
 SEC63_fwd (5'-CCGTGAAGAAAGGGAGTTTCG-3')
 SEC63_rev (5'-CCTGAACGGCCATCTGAGAA-3')
 JUN_fwd (5'-GAGCTGGAGCGCCTGATAAT-3')
 JUN_rev (5'-CCCTCTGCTCATCTGTCC-3')
 EDNRB_fwd (5'-AAAGCAGAGACGGGAAGTGG-3')
 EDNRB_rev (5'-CTGCTGAGGTGAAGGGGAAG-3')
 β-actin (mouse)_fwd (5'-CCTCTATGCCAACACAGTGC-3')
 β-actin (mouse)_rev (5'-ACATCTGCTGGAAGGTGGAC-3')
 Hmga1 (mouse)_fwd (5'-CAAGACCCGAAAGTACCA-3')
 Hmga1 (mouse)_rev (5'-ATGCCCTCTCTCTCCTT-3')
 Hmga2 (mouse)_fwd (5'-ACCCAGAGGAAGACCCAAA-3')
 Hmga2 (mouse)_rev (5'-CCTCTTGGCCGTTTTTCTCCA-3')

miRNA was extracted using an MiRcute miRNA Extraction and Separation Kit (Tiangen, Beijing, China), then synthesized with an MiRcute Enhanced miRNA cDNA First Strand Synthesis Kit (Tiangen). Real-time PCR was carried out on an QuantStudio™ 3 Realtime-PCR Instrument using MiRcute Enhanced miRNA Fluorescence Quantification Kit (SYBR Green; Tiangen). All experiments were carried out in accordance with the manufacturers' instructions. U6 was used as an internal control. The primer sequences for PCR were as follows:

U6_fwd (5'-CTCGCTTCGGCAGCAC-3')
 novel-miR-27_fwd (5'-TGTCTGTTTCTCCTG-3')
 novel-miR-72_fwd (5'-CTGATCTGGCTGGCTAGGT-3')
 novel-miR-4_fwd (5'-CGTCCTCCCCCTCCCCG-3')

miR-18a-3p_fwd (5'-ACTGCCCTAAGTGCTCCTTCTGG-3')
 novel-miR-68_fwd (5'-GTGCCTGTAGTCCAGCT-3')
 novel-miR-50_fwd (5'-CTGCGTCTTTGTGCTTTA-3')
 novel-miR-63_fwd (5'-CGGGTGCTGTAGGCTTT-3')
 miR-3656_fwd (5'-GGCGGTGCGGGGGTGG-3')
 miR-59_fwd (5'-CCCTCTCTCTCCCCCT-3')

High-throughput sequencing and bioinformatics analysis of miRNAs

CRL-1474 cells were transfected with Vector Ctrl or Flag-progerin for 9 days. Total RNA was isolated using Trizol reagent. The miRNA libraries were constructed using a VAHTSTM Small RNA Library Prep Kit for Illumina (Vazyme, Nanjing, China). miRNAs were first ligated with a 5' RNA adaptor, then a 3' RNA adaptor. After first-strand synthesis and PCR amplification, the final bands were purified and submitted for sequencing on an Illumina HiSeq2500 analyzer. Sequencing was performed at Biomarker Technologies (Beijing, China). All raw miRNA-seq reads were mapped to the human genome (hg19). A cut-off *P*-value < 0.05 and absolute values of log₂-fold changes > 1.5 were used for differential miRNA expression analysis.

High-throughput sequencing and bioinformatics analysis of the transcriptome

Progerin-expressing CRL-1474 cells were transfected with Vector Ctrl or His-HMGA1 for 9 days. Total RNA was isolated using Trizol reagent. The RNA-Seq libraries were constructed using a VAHTS Universal V6 RNA-seq Library Prep Kit (Vazyme) for Illumina and sequenced on an Illumina HiSeq 2500 at Biomarker Technologies. All raw RNA-seq reads were mapped to the human genome (hg19) with TopHat coupled with Bowtie 2 and default parameters. Transcriptomes were assembled and fragments per kilo-base per million reads for each gene were computed with Cufflinks. A cut-off *P*-value < 0.05 and absolute values of log₂-fold changes > 1 were used for differential gene expression analysis.

Plasmids and antibodies

The following vectors were used in this study: pCDH-CMV-3 × Flag-progerin; pCDH-CMV-3 × Flag-HMGA1; pCDH-CMV-His-HMGA1; pCDH-CMV-3 × Flag-HMGA2; pCDH-CMV-HA-HMGA2; pCDH-CMV-CDK7; pGEX-6P1-HMGA1; pGEX-6P1-truncated-HMGA1 (1–89); pGEX-6P1-truncated-HMGA1 (1–63); pGEX-6P1-truncated-HMGA1 (23–107); pGEX-6P1-truncated-HMGA1 (32–107); pGEX-6P1-HMGA2; pGL3-HMGA1-3'-UTR; pGL3-HMGA2-3'-UTR; mutant pGL3-HMGA1-3'-UTR-mut and pGL3-HMGA2-3'-UTR-mut; pGL3-Hmga1-3'-UTR; pGL3-Hmga2-3'-UTR; mutant: pGL3-Hmga1-3'-UTR-mut and pGL3-HMGA2-3'-UTR-mut; and pmR-mCherry-miR-59. Additionally, shHMGA1#1, shHMGA1#2, shHMGA2#1, and shHMGA2#2 oligonucleotides were designed and cloned into the lentiviral RNAi system (pLKO.1). The sequences of shRNAs, which were designed to target human genes, were as follows:

shCtrl_fwd (5'-CCGGAATGCCTACGTAAAGCTATACCTCGAGGTATAGCTTAACGTAGGCATTTTTTTG-3') and shCtrl_rev (5'-AATTCAAAAAATGCCTACGTAAAGCTATACCTCGAGGTATAGCTTAACGTA

GGCATT-3'); shHMGA1#1_fwd (5'-CCGGCAACTCCAGGAAGGAAACCAACTCGAGTTGGTTTCCTTCTGGAGTTGTTTTT-3') and shHMGA1#1_rev (5'-AATTCAAAAAACAACCTCCAGGAAGGAAACCAACTCGAGTTGGTTTCCTTCTGGAGTTG-3'); shHMGA1#2_fwd (5'-CCGGCCTTGGCCTCCAAGCAGGAACTCGAGTTTCTGCTTGGAGGCCAAGGTTT-3') and shHMGA1#2_rev (5'-AATTCAAAAAACCTTGGCCTCCAAGCAGGAACTCGAGTTTCTGCTTGGAGGCCAAGG-3'); shHMGA2#1_fwd (5'-CCGGAGTCCCTCTAAAGCAGCTCAACTCGAGTTGAGCTGCTTAGAGGGACT-3') and shHMGA2#1_rev (5'-AATTCAAAAAAGTCCCTCTAAAGCAGCTCAACTCGAGTTGAGCTGCTTAGAGGGACT-3'); shHMGA2#2_fwd (5'-CCGGAGGAGGAACTGAAGAGACATCTCGAGATGTCTTTCAGTTTCTCTTTTTT-3') and shHMGA2#2_rev (5'-AATTCAAAAAAGGAGGAACTGAAGAGACATCTCGAGATGTCTTTCAGTTTCTCTCT-3').

siCDK7#1 and siCDK7#2 were designed and purchased from Gemma Biology (Shanghai, China).

siCtrl_fwd (5'-UUCUCCGAACGUGUCACGUTT-3') and siCtrl_rev (5'-ACGUGACACGUUCGGAGAATT-3'); siCDK7#1_fwd (5'-GCCAGAGUAAGAACCATT-3') and siCDK7#1_rev (5'-UGGUGUUCUUAUCUCUGGCTT-3'); siCDK7#2_fwd (5'-GACUCUUAAGGAUUAGAATT-3') and siCDK7#2_rev (5'-UUCUUAUCCUUGAAGAUUCTT-3').

The following antibodies were used: antibodies against progerin (ab66587; Abcam); HMGA1 (#7777 for WB; Cell Signaling Technology, ab4078 for CHIP; and ab129153 for IHC; Abcam); HMGA2 (#8179 for WB; Cell Signaling Technology and GB111395 for IHC; Servicebio, Wuhan, China); β-actin (A1978; Sigma, St. Louis, MO, USA); Ki67 (GTX16667; GeneTex); lamin B1 (ab16048; Abcam); cyclin A2 (ab181591; Abcam); Flag (M20008; Abmart); His (M30111; Abmart); HA (SAB2702196; Sigma); RNAPII (ab817; Abcam); XPB (ab190698; Abcam); CDK7 (2916S; Cell Signaling Technology); TFIIH4 (DF8857; Affinity); RNAPII Ser2P (ab5095; Abcam); and RNAPII Ser5P (ab193467; Abcam). Normal mouse IgG (Santa Cruz Biotechnology, sc-2025), normal rabbit IgG (CST, #2729), secondary goat anti-mouse, and goat anti-rabbit antibodies were obtained from ZSGB-BIO (Beijing, China).

Lentiviral production and infection

The lentivirus packaging vectors used were pMDlg/pRRE, VSV-G, and pRSV-Rev. Generation of lentivirus in HEK293T cells and transfection of lentiviral constructs into recipient cell lines were performed following the manufacturer's instructions (Thermo). The transfection reagent, polyethylenimine (PEI), was purchased from Sigma.

miRNAs transfection

miRs and anti-miRs (Gemma Biology) were transfected into fibroblasts using Lipofectamine 2000 (Invitrogen) according to manufacturer's instructions.

Western blotting and immunoprecipitation

Cells were collected and washed three times with cold PBS and lysed in 1 × Laemmli sample buffer. The supernatant was subjected to SDS-PAGE, followed by transferred onto PVDF membranes (Millipore), and detected using ECL reagents (GE Healthcare, Buckinghamshire, United Kingdom).

Immunoprecipitation assays were performed as previously described (Zhao *et al.*, 2015).

Luciferase reporter assays

Wild-type and mutated HMGA1 and HMGA2 3'UTR (human and mouse) sequences were PCR-amplified from cDNA using specific primers. The wild-type (WT) or mutant (MT) 3'UTRs were cloned into the pGL3-promoter vector. The precursor sequence of miR-59 was PCR-amplified from cDNA using specific primers. The sequence of pre-miR-59 was cloned into the pmR-mCherry vector. For luciferase reporter assays, HEK293T cells were co-transfected with the indicated 3'UTR luciferase reporter vectors and pmR-mCherry-miR-59 for 48 h. The relative luciferase activities were measured using a Dual Luciferase Reporter Assay Kit (E1910; Promega). The primer sequences were as follows:

WT HMGA1 3'UTR_fwd (5'-GCTCTAGATAGTCCCGTACTAGGTTGA-3') and WT HMGA1 3'UTR_rev (5'-ACCGCCGCGCCAGAAAA GGATATTTTTTTTATTC-3'); mutated HMGA1 3'UTR site 1_fwd (5'-TTTGTGGGAAACACCGGCTGGGGCAT-3') and mutated HMGA1 3'UTR site 1_rev (5'-ATGCCCCAGCCGTGTTCCCCACAAA-3'); mutated HMGA1 3'UTR site 2_fwd (5'-AGAGTGAGCAACGCCGCC AAATCGA-3') and mutated HMGA1 3'UTR site 2_rev (5'-TCGATTT GGGCGGCGTTGCTCACTCT-3'); WT HMGA2 3'UTR_fwd (5'-GCTC TAGATGGGAGAAAATCACATAACC-3') and WT HMGA2 3'UTR_rev (5'-ACCGCCGCGCAAGAAGTGCAGATGATTAGAATCAC-3'); mutated HMGA2 3'UTR site 1_fwd (5'-GCAAAAAAAAAAAGCGCCGG CAATCTCTCTC-3') and mutated HMGA2 3'UTR site 1_rev (5'-GAG AGAGATTGCCCGCGCTTTTTTTTTTTGTC-3'); mutated HMGA2 3'UTR site 2_fwd (5'-CACCTAATTATGAGCTCCGAGGAGCGAAATC-3'); mutated HMGA2 3'UTR site 2_rev (5'-GATTTTCGCTCCTCGGAGCT CATAATTAGGTG-3'); WT Hmga1 3'UTR (mouse)_fwd (5'-GCT CTAGAGCATGTCCCAACAAAG-3') and WT Hmga1 3'UTR (mouse) _rev (5'-ACCGCCGCGCGTAACTGCAAATAAGAAACCA-3'); mutated Hmga1 3'UTR site 1 (mouse)_fwd (5'-GGGGAAGCGCCGCTGGGGC GCAG-3') and mutated Hmga1 3'UTR site 1 (mouse)_rev (5'-CTG CGCCCCAGCGCGCTTCCCC-3'); mutated Hmga1 3'UTR site 2 (mouse)_fwd (5'-CCTTGTTCTGTGCGCCAGGG-3') and mutated Hmga1 3'UTR site 2 (mouse)_rev (5'-ACCGCCGCGCAATACTGG CCACCCTGGCGCACAG-3'); WT Hmga2 3'UTR (mouse)_fwd (5'-GC TCTAGAGACTGCAGTGACCAGTT-3') and WT Hmga2 3'UTR (mouse)_rev (5'-ACCGCCGCGCAAATAGTGTCTTTATATAGCAA-3'); mutated Hmga2 3'UTR site 1 (mouse)_fwd (5'-AACACGCGCCACA CAGTTTAAACAAT-3') and mutated Hmga2 3'UTR site 1 (mouse)_rev (5'-ATTGTTAAACTGTGTGGCGGTGTT-3'); mutated Hmga2 3'UTR site 2 (mouse) _rev (5'-ACCGCCGCGCGTTTCGCTGGTGCATGT CATC-3'). pmR-mCherry-miR-59_fwd (5'-CCGCTCGAGCTCTGGAGC ATCCAGGC-3') and pmR-mCherry-miR-59_rev (5'-CGAATTCC TTCTACATTTGGAGCTGAC-3').

MS analysis

Flag-HMGA1 protein was purified from Flag-HMGA1-HEK293T cells and was then resolved by 12% SDS-PAGE. After Coomassie brilliant blue staining, the band of Ctrl or Flag-HMGA1 was excised for liquid chromatography-tandem mass spectrometry (LC-MS/MS) analysis,

which was performed in the Institute of Biophysics (Chinese Academy of Sciences, Beijing, China).

Chromatin immunoprecipitation-quantitative PCR

Cells were collected and treated with the formaldehyde cross-linking method (Lin *et al.*, 2020).ChIP experiments were carried out in accordance with the manufacturer's instructions (17-10086; Millipore). Immunoprecipitated DNA was amplified with primers on an QuantStudio™ 3 Realtime-PCR Instrument. The primer sequences for PCR, which were synthesized by Comate Bioscience (Changchun, China), were as follows:

CCNA2 (TSS)_fwd (5'-AAATGATAGTCGCCAAAGTTTA-3')
 CCNA2 (TSS)_rev (5'-AGTATCCCAGACTATTGAAATGGA-3')
 CCNB1 (TSS)_fwd (5'-ATCGCCCTGGAAACGCATTCTCTG-3')
 CCNB1 (TSS)_rev (5'-ACCAGCCAAGGACCTACACCCAGCA-3')
 CDK1 (TSS)_fwd (5'-GTAGCTGGGCTCTGATTGGCTG-3')
 CDK1 (TSS)_rev (5'-CTTATTATCCGCGGCGGCC-3')
 CDC6 (TSS)_fwd (5'-GTGACTACAGCCAATCAGAATCGAG-3')
 CDC6 (TSS)_rev (5'-TGCAGGATCCTTCTCACGTCTCTCA-3')
 CDC25A (TSS)_fwd (5'-GCCGCTATTACCGCGAAAGG-3')
 CDC25A (TSS)_rev (5'-AACCTGAAGATTAATCCAAACAAA-3')
 ORC1 (TSS)_fwd (5'-CCTATCGAATCAATGATGGCGG-3')
 ORC1 (TSS)_rev (5'-AGAAATGAAAAGAAGGTGGAAGGA-3')
 PLK1 (TSS)_fwd (5'-TCTATGAACAATTATAATATGTACA-3')
 PLK1 (TSS)_rev (5'-TCTGATCCTTCATAGAGCCAGC-3')
 PLK1 (TSS)_fwd (5'-GGATCGTGGTACTGCTATGGCGGT-3')
 PLK1 (TSS)_rev (5'-AGATGGCGCCCAATAAGTATGTGTG-3')

GST fusion protein purification and GST bead pull down

Briefly, the expression of GST, GST-HMGA1, truncated-GST-HMGA1, and GST-HMGA2 protein was induced by adding 0.1 mmol/l IPTG at 16°C for 16 h with shaking, followed by purification on glutathione Sepharose beads, according to the manufacturer's instructions (GE Healthcare).

Virus production

The antisense oligonucleotide of novel-miR-59 was packaged into AAV serotypes 9 vectors with a mCherry reporter (GeneChem, Shanghai, China). The expression of anti-miRNA and mCherry was driven by U6 and CAG promoters, respectively.

The antisense oligonucleotide sequence of miR-59:

5'-AGGGGGGAGAGAGAGAGGG-3'

Construction of *Lmna*^{G609G/G609G} mice model

All animal experiments were approved by Ethics Committee of School of Life Sciences, Northeast Normal University, China (AP20191012). The HGPS mouse model (ICR background), carrying the *Lmna*^{G609G}, was generated by the BE4-Gam system. The protocols for the BE4-Gam system and microinjection of pronuclear-stage embryos have been described in detail in published protocols (Song *et al.*, 2016; Liu *et al.*, 2018). Briefly, a mixture of BE4-Gam mRNA (200 ng/μl) and sgRNA-*Lmna* (30 ng/μl) was co-injected into the

cytoplasm of pronuclear-stage embryos of mice. The injected embryos were transferred to embryo culture medium for 30–60 min, followed by transferring the injected embryos into the recipient mother. The embryos continue to develop, and the founder mice (referred to as F0) were born: wild-type mice ($Lmna^{+/+}$), heterozygous mice ($Lmna^{G609G/+}$), and homozygous mice ($Lmna^{G609G/G609G}$). F1 heterozygous mice ($Lmna^{G609G/+}$) were obtained by crossing F0 heterozygous mice ($Lmna^{G609G/+}$). F2 homozygous mice ($Lmna^{G609G/G609G}$) were obtained by crossing F1 heterozygous mice ($Lmna^{G609G/+}$). We selected F2 WT mice and homozygous mice for subsequent experiments. The mice were housed with a 12 h light/dark cycle between 06:00 and 18:00 in a temperature-controlled room ($22 \pm 1^\circ\text{C}$). Water and rodent feed were fed *ad libitum*.

sgRNA-*Lmna* oligo sequences used: GTGGGCGGATCCATC TCCTC. Genotypes of newborn mice were identified using a Mouse Direct PCR kit (B40015; Bimake). The sequences of PCR primers to test genotypes were listed as follows:

mLmna_fwd: CGAAGGCTTCCTGGCTATTT

mLmna_rev: TGCTGTAGGCAGAGATGA

AAV9-mCherry-anti-miR-59 virus injection of mice

For AAV injection, 8-day-old $Lmna^{G609G/G609G}$ mice were injected intraperitoneally with either AAV9-mCherry-anti-miR-control or AAV9-mCherry-anti-miR-59, and wide-type mice were injected with AAV9-mCherry-anti-miR-control. Each mouse was injected with 5×10^{11} viral particles in 100 μl of PBS. Experiments were done in a non-blind fashion since HGPS mouse have overt phenotype.

Imaging in small animals

Eight-day-old $Lmna^{G609G/G609G}$ mice were injected intraperitoneally with PBS or AAV9-mCherry-anti-miR-59. Thirty days after injection, detection of the mCherry signal was obtained with a lumina small animal imager (IVIS® Lumina III; PerkinElmer). The mice were injected with pentobarbital sodium, and all hair was shaved to facilitate photography before the organs were extracted for imaging.

Open field experiments in mice

The animals were acclimatized to the testing room for at least 1 h before the test. Before each individual mouse trial, the testing apparatus was cleaned with 75% ethanol. A curtain surrounded the equipment to prevent interference and to create a uniform environment. Wide-type and $Lmna^{G609G/G609G}$ mice, which were treated with AAV9-mCherry-anti-miR-Ctrl or AAV9-mCherry-anti-miR-59, were carried out for open field experiments. The movement distance and trail were recorded and analyzed for 20 min after the mice adapted to the environment using Ethovision XT 10 (Noldus, Wageningen, The Netherlands).

Histologic analysis

For the histologic analyses, 14-week-old mice of the indicated genotypes were first perfused with PBS, then with 4% paraformaldehyde (PFA). Whole organs were incubated in 4% PFA at 4°C for 3 days. All the samples were embedded in paraffin and sectioned. The

sections were analyzed with hematoxylin and eosin staining ([H&E], 9217; Absin, Shanghai, China) and Masson staining (9347; Absin). H&E staining was performed in skin, and fat layer thickness (always the same region) was blindly calculated on five random fields per mouse, three measurements were randomly selected in each section. Masson staining in mouse tissues showing interstitial fibrosis in the heart and quadriceps muscle, and interstitial fibrosis was quantified on five random fields per tissue. Masson staining in mouse tissues showing adventitial width, and adventitial width was quantified on five random fields per mouse. The fat layer thickness and adventitial width and the fibrosis in heart and muscle were calculated by Image J, unpaired Student's *t*-test.

The IHC staining was performed by Servicebio. Tissues of mice were stained with antibodies against HMGA1 and HMGA2, the proportion of positive cells was used to quantify the expression of protein in tissues.

Statistical analysis

Data were compiled from at least three independent replicate experiments. Data are presented as the mean \pm SD ($*P < 0.05$, $**P < 0.01$, and $***P < 0.001$). $P < 0.05$ was considered statistically significant. Statistical parameters and methods are reported in the figures. Unless specified, comparisons between groups were made using an unpaired two-tailed Student's *t*-test. Statistical analysis was carried out using the GraphPad Prism software (GraphPad Software, La Jolla, CA, USA).

Data availability

Any data and materials that can be shared will be released via a Data/Material sharing Agreement. All requests should be made to the primary or corresponding authors. miRNA-seq data and RNA-seq data generated in the present study were deposited in the NCBI SRA (no. PRJNA817648 and no. PRJNA817844). No. [PRJNA817648](https://www.ncbi.nlm.nih.gov/sra/PRJNA817648). No. [PRJNA817844](https://www.ncbi.nlm.nih.gov/sra/PRJNA817844).

Expanded View for this article is available [online](#).

Acknowledgments

This work was supported by the grants from the National Natural Science Foundation of China (grant numbers: 32171163, 32071292, 31771335, 31870765, and 31770825) and Research Grants of Jilin Science and Technology (grant numbers: 20200404106YY) and Jilin Development and Reform (<http://jldrc.jl.gov.cn/>).

Author contributions

Yu Zhang: Conceptualization; formal analysis; supervision; funding acquisition; writing—original draft; project administration; writing—review and editing. **Qianying Hu:** Resources; data curation; software; formal analysis; validation; investigation; visualization; methodology; writing—original draft; project administration; writing—review and editing. **Na Zhang:** Formal analysis; validation; investigation; methodology; writing—original draft. **Tingting Sui:** Resources; formal analysis. **Guanlin Li:** Validation. **Zhiyao Wang:** Software; validation. **Mingyue Liu:** Software. **Xiaojuan Zhu:** Formal analysis; funding acquisition; methodology; writing—original draft. **Baiqu Huang:** Conceptualization; funding acquisition; investigation; writing—

original draft; writing—review and editing. **Jun Lu:** Conceptualization; formal analysis; funding acquisition; writing—original draft; writing—review and editing. **Zhanjun Li:** Resources; methodology; writing—original draft.

Disclosure and competing interests statement

The authors declare that they have no conflict of interest.

References

- Akhtar MS, Heidemann M, Tietjen JR, Zhang DW, Chapman RD, Eick D, Ansari AZ (2009) TFIIF kinase places bivalent marks on the carboxy-terminal domain of RNA polymerase II. *Mol Cell* 34: 387–393
- Babar IA, Cheng CJ, Booth CJ, Liang X, Weidhaas JB, Saltzman WM, Slack FJ (2012) Nanoparticle-based therapy in an *in vivo* microRNA-155 (miR-155)-dependent mouse model of lymphoma. *Proc Natl Acad Sci USA* 109: E1695–E1704
- Bartel DP (2004) microRNAs: genomics, biogenesis, mechanism, and function. *Cell* 116: 281–297
- Battista S, Pentimalli F, Baldassarre G, Fedele M, Fidanza V, Croce CM, Fusco A (2003) Loss of Hmga1 gene function affects embryonic stem cell lympho-hematopoietic differentiation. *FASEB J* 17: 1496–1498
- Beuret E, Liao HK, Yamamoto M, Hernandez-Benitez R, Fu Y, Erikson G, Reddy P, Izpisua Belmonte JC (2019) Single-dose CRISPR-Cas9 therapy extends lifespan of mice with Hutchinson-Gilford progeria syndrome. *Nat Med* 25: 419–422
- Buchwalter A, Hetzer MW (2017) Nucleolar expansion and elevated protein translation in premature aging. *Nat Commun* 8: 328
- Calin GA, Cimmino A, Fabbri M, Ferracin M, Wojcik SE, Shimizu M, Taccioli C, Zanesi N, Garzon R, Aqeilan RI et al (2008) MiR-15a and miR-16-1 cluster functions in human leukemia. *Proc Natl Acad Sci USA* 105: 5166–5171
- Cao K, Graziotto JJ, Blair CD, Mazzulli JR, Erdos MR, Krainc D, Collins FS (2011) Rapamycin reverses cellular phenotypes and enhances mutant protein clearance in Hutchinson-Gilford progeria syndrome cells. *Sci Transl Med* 3: 89ra58
- Cenni V, Capanni C, Mattioli E, Schena E, Squarzone S, Bacalini MG, Garagnani P, Salvioli S, Franceschi C, Lattanzi G (2020) Lamin A involvement in ageing processes. *Ageing Res Rev* 62: 101073
- Cheng Y, Zhang C (2010) microRNA-21 in cardiovascular disease. *J Cardiovasc Transl Res* 3: 251–255
- Chlamydas S, Holz H, Samata M, Chelmicki T, Georgiev P, Pelechano V, Dündar F, Dasmeh P, Mittler G, Cadete FT et al (2016) Functional interplay between MSL1 and CDK7 controls RNA polymerase II Ser5 phosphorylation. *Nat Struct Mol Biol* 23: 580–589
- Dhillon S (2021) Lonafarnib: first approval. *Drugs* 81: 283–289
- Eilebrecht S, Benecke BJ, Benecke A (2011) 7SK snRNA-mediated, gene-specific cooperativity of HMGA1 and P-TEFb. *RNA Biol* 8: 1084–1093
- Erdos MR, Cabral WA, Tavarez UL, Cao K, Gvozdenovic-Jeremic J, Narisu N, Zervas PM, Crumley S, Boku Y, Hanson G et al (2021) A targeted antisense therapeutic approach for Hutchinson-Gilford progeria syndrome. *Nat Med* 27: 536–545
- Eriksson M, Brown WT, Gordon LB, Glynn MW, Singer J, Scott L, Erdos MR, Robbins CM, Moses TY, Berglund P et al (2003) Recurrent de novo point mutations in lamin A cause Hutchinson-Gilford progeria syndrome. *Nature* 423: 293–298
- Foti D, Chiefari E, Fedele M, Iuliano R, Brunetti L, Paonessa F, Manfioletti G, Barbetti F, Brunetti A, Croce CM et al (2005) Lack of the architectural factor HMGA1 causes insulin resistance and diabetes in humans and mice. *Nat Med* 11: 765–773
- Glover-Cutter K, Larochelle S, Erickson B, Zhang C, Shokat K, Fisher RP, Bentley DL (2009) TFIIF-associated Cdk7 kinase functions in phosphorylation of C-terminal domain Ser7 residues, promoter-proximal pausing, and termination by RNA polymerase II. *Mol Cell Biol* 29: 5455–5464
- Gonzalo S, Kreienkamp R, Askjaer P (2017) Hutchinson-Gilford progeria syndrome: a premature aging disease caused by LMNA gene mutations. *Ageing Res Rev* 33: 18–29
- Gordon LB, Massaro J, D'Agostino RB Sr, Campbell SE, Brazier J, Brown WT, Kleinman ME, Kieran MW (2014a) Impact of farnesylation inhibitors on survival in Hutchinson-Gilford progeria syndrome. *Circulation* 130: 27–34
- Gordon LB, Rothman FG, López-Otín C, Misteli T (2014b) Progeria: a paradigm for translational medicine. *Cell* 156: 400–407
- Joo YJ, Ficarro SB, Chun Y, Marto JA, Buratowski S (2019) *In vitro* analysis of RNA polymerase II elongation complex dynamics. *Genes Dev* 33: 578–589
- Jopling CL, Yi M, Lancaster AM, Lemon SM, Sarnow P (2005) Modulation of hepatitis C virus RNA abundance by a liver-specific microRNA. *Science* 309: 1577–1581
- Jung HJ, Coffinier C, Choe Y, Beigneux AP, Davies BS, Yang SH, Barnes RH 2nd, Hong J, Sun T, Pleasure SJ et al (2012) Regulation of prelamin A but not lamin C by miR-9, a brain-specific microRNA. *Proc Natl Acad Sci USA* 109: E423–E431
- Kubben N, Misteli T (2017) Shared molecular and cellular mechanisms of premature ageing and ageing-associated diseases. *Nat Rev Mol Cell Biol* 18: 595–609
- Kuper J, Kisker C (2021) Three targets in one complex: a molecular perspective of TFIIF in cancer therapy. *DNA Repair (Amst)* 105: 103143
- Lin C, Li H, Liu J, Hu Q, Zhang S, Zhang N, Liu L, Dai Y, Cao D, Li X et al (2020) Arginine hypomethylation-mediated proteasomal degradation of histone H4—an early biomarker of cellular senescence. *Cell Death Differ* 27: 2697–2709
- Ling H, Fabbri M, Calin GA (2013) microRNAs and other non-coding RNAs as targets for anticancer drug development. *Nat Rev Drug Discov* 12: 847–865
- Liu B, Wang J, Chan KM, Tjia WM, Deng W, Guan X, Huang JD, Li KM, Chau PY, Chen DJ et al (2005) Genomic instability in laminopathy-based premature aging. *Nat Med* 11: 780–785
- Liu Z, Chen M, Chen S, Deng J, Song Y, Lai L, Li Z (2018) Highly efficient RNA-guided base editing in rabbit. *Nat Commun* 9: 2717
- Luna JM, Scheel TK, Danino T, Shaw KS, Mele A, Fak JJ, Nishiuchi E, Takacs CN, Catanese MT, de Jong YP et al (2015) Hepatitis C virus RNA functionally sequesters miR-122. *Cell* 160: 1099–1110
- Mariño G, Ugalde AP, Fernández AF, Osorio FG, Fueyo A, Freije JM, López-Otín C (2010) Insulin-like growth factor 1 treatment extends longevity in a mouse model of human premature aging by restoring somatotroph axis function. *Proc Natl Acad Sci USA* 107: 16268–16273
- Maurer B, Stanczyk J, Jünger A, Akhmetshina A, Trenkmann M, Brock M, Kowal-Bielecka O, Gay RE, Michel BA, Distler JH et al (2010) microRNA-29, a key regulator of collagen expression in systemic sclerosis. *Arthritis Rheum* 62: 1733–1743
- Narita M, Narita M, Krizhanovsky V, Nuñez S, Chicas A, Hearn SA, Myers MP, Lowe SW (2006) A novel role for high-mobility group proteins in cellular senescence and heterochromatin formation. *Cell* 126: 503–514
- Nishino J, Kim I, Chada K, Morrison SJ (2008) Hmga2 promotes neural stem cell self-renewal in young but not old mice by reducing p16Ink4a and p19Arf Expression. *Cell* 135: 227–239
- Nissan X, Blondel S, Navarro C, Maury Y, Denis C, Girard M, Martinat C, De Sandre-Giovannoli A, Levy N, Peschanski M (2012) Unique preservation of

- neural cells in Hutchinson-Gilford progeria syndrome is due to the expression of the neural-specific miR-9 microRNA. *Cell Rep* 2: 1–9
- Osorio FG, Navarro CL, Cadiñanos J, López-Mejía IC, Quirós PM, Bartoli C, Rivera J, Tazi J, Guzmán G, Varela I et al (2011) Splicing-directed therapy in a new mouse model of human accelerated aging. *Sci Transl Med* 3: 106ra107
- Pendás AM, Zhou Z, Cadiñanos J, Freije JM, Wang J, Hultenby K, Astudillo A, Wernerson A, Rodríguez F, Tryggvason K et al (2002) Defective prelamin A processing and muscular and adipocyte alterations in Zmpste24 metalloproteinase-deficient mice. *Nat Genet* 31: 94–99
- Penzo C, Arnoldo L, Pegoraro S, Petrosino S, Ros G, Zanin R, Wiśniewski JR, Manfioletti G, Sgarra R (2019) HMGA1 modulates gene transcription sustaining a tumor signalling pathway acting on the epigenetic status of triple-negative breast cancer cells. *Cancers (Basel)* 11: 1105–1131
- Prakash A, Gordon LB, Kleinman ME, Gurary EB, Massaro J, D'Agostino R Sr, Kieran MW, Gerhard-Herman M, Smoot L (2018) Cardiac abnormalities in patients with Hutchinson-Gilford progeria syndrome. *JAMA Cardiol* 3: 326–334
- Puttaraju M, Jackson M, Klein S, Shilo A, Bennett CF, Gordon L, Rigo F, Misteli T (2021) Systematic screening identifies therapeutic antisense oligonucleotides for Hutchinson-Gilford progeria syndrome. *Nat Med* 27: 526–535
- Roggli E, Gattesco S, Caille D, Briet C, Boitard C, Meda P, Regazzi R (2012) Changes in microRNA expression contribute to pancreatic β -cell dysfunction in prediabetic NOD mice. *Diabetes* 61: 1742–1751
- Rupaimoole R, Slack FJ (2017) microRNA therapeutics: towards a new era for the management of cancer and other diseases. *Nat Rev Drug Discov* 16: 203–222
- Santiago-Fernández O, Osorio FG, Quesada V, Rodríguez F, Basso S, Maeso D, Rolas L, Barkaway A, Nourshargh S, Folgueras AR et al (2019) Development of a CRISPR/Cas9-based therapy for Hutchinson-Gilford progeria syndrome. *Nat Med* 25: 423–426
- Sgarra R, Pegoraro S, Ros G, Penzo C, Chiefari E, Foti D, Brunetti A, Manfioletti G (2018) High Mobility Group A (HMGA) proteins: molecular instigators of breast cancer onset and progression. *Biochim Biophys Acta Rev Cancer* 1869: 216–229
- Sharma P, Yadav P, Jain RP, Bera AK, Karunakaran D (2022) miR-142-3p simultaneously targets HMGA1, HMGA2, HMGB1, and HMGB3 and inhibits tumorigenic properties and in-vivo metastatic potential of human cervical cancer cells. *Life Sci* 291: 120268
- Shiekhattar R, Mermelstein F, Fisher RP, Drapkin R, Dynlacht B, Wessling HC, Morgan DO, Reinberg D (1995) Cdk-activating kinase complex is a component of human transcription factor TFIIH. *Nature* 374: 283–287
- Song Y, Yuan L, Wang Y, Chen M, Deng J, Lv Q, Sui T, Li Z, Lai L (2016) Efficient dual sgRNA-directed large gene deletion in rabbit with CRISPR/Cas9 system. *Cell Mol Life Sci* 73: 2959–2968
- Teng K, Wei S, Zhang C, Chen J, Chen J, Xiao K, Liu J, Dai M, Guan X, Yun J et al (2019) KIFC1 is activated by TCF-4 and promotes hepatocellular carcinoma pathogenesis by regulating HMGA1 transcriptional activity. *J Exp Clin Cancer Res* 38: 329
- Ugalde AP, Ramsay AJ, de la Rosa J, Varela I, Mariño G, Cadiñanos J, Lu J, Freije JM, López-Otín C (2011) Aging and chronic DNA damage response activate a regulatory pathway involving miR-29 and p53. *EMBO J* 30: 2219–2232
- Vignali R, Marracci S (2020) HMGA genes and proteins in development and evolution. *Int J Mol Sci* 21: 654
- Wang D, Tai PWL, Gao G (2019) Adeno-associated virus vector as a platform for gene therapy delivery. *Nat Rev Drug Discov* 18: 358–378
- Wei J, Hao Q, Chen C, Li J, Han X, Lei Z, Wang T, Wang Y, You X, Chen X et al (2020) Epigenetic repression of miR-17 contributed to di(2-ethylhexyl) phthalate-triggered insulin resistance by targeting Keap1-Nrf2/miR-200a axis in skeletal muscle. *Theranostics* 10: 9230–9248
- Xiong XD, Jung HJ, Gombar S, Park JY, Zhang CL, Zheng H, Ruan J, Li JB, Kaeberlein M, Kennedy BK et al (2015) microRNA transcriptome analysis identifies miR-365 as a novel negative regulator of cell proliferation in Zmpste24-deficient mouse embryonic fibroblasts. *Mutat Res* 777: 69–78
- Yan C, Dodd T, He Y, Tainer JA, Tsutakawa SE, Ivanov I (2019) Transcription preinitiation complex structure and dynamics provide insight into genetic diseases. *Nat Struct Mol Biol* 26: 397–406
- Yu KR, Park SB, Jung JW, Seo MS, Hong IS, Kim HS, Seo Y, Kang TW, Lee JY, Kurtz A et al (2013) HMGA2 regulates the *in vitro* aging and proliferation of human umbilical cord blood-derived stromal cells through the mTOR/p70S6K signaling pathway. *Stem Cell Res* 10: 156–165
- Zhang CL, Liu X, He QJ, Zheng H, Xu S, Xiong XD, Yuan Y, Ruan J, Li JB, Xing Y et al (2017) miR-342-5p promotes Zmpste24-deficient mouse embryonic fibroblasts proliferation by suppressing GAS2. *Mol Med Rep* 16: 8944–8952
- Zhao L, Zhang Y, Gao Y, Geng P, Lu Y, Liu X, Yao R, Hou P, Liu D, Lu J et al (2015) JMJD3 promotes SAHF formation in senescent WI38 cells by triggering an interplay between demethylation and phosphorylation of RB protein. *Cell Death Differ* 22: 1630–1640



License: This is an open access article under the terms of the [Creative Commons Attribution-NonCommercial-NoDerivs](https://creativecommons.org/licenses/by-nc-nd/4.0/) License, which permits use and distribution in any medium, provided the original work is properly cited, the use is non-commercial and no modifications or adaptations are made.